

**Original citation:**

Boon, C. W., Houlsby, G. T. and Utili, Stefano. (2015) Designing tunnel support in jointed rock masses via the DEM. *Rock Mechanics and Rock Engineering*, 48 (2). pp. 603-632. <http://dx.doi.org/10.1007/s00603-014-0579-8>

**Permanent WRAP url:**

<http://wrap.warwick.ac.uk/65717>

**Copyright and reuse:**

The Warwick Research Archive Portal (WRAP) makes this work by researchers of the University of Warwick available open access under the following conditions. Copyright © and all moral rights to the version of the paper presented here belong to the individual author(s) and/or other copyright owners. To the extent reasonable and practicable the material made available in WRAP has been checked for eligibility before being made available.

Copies of full items can be used for personal research or study, educational, or not-for profit purposes without prior permission or charge. Provided that the authors, title and full bibliographic details are credited, a hyperlink and/or URL is given for the original metadata page and the content is not changed in any way.

**Publisher's statement:**

"The final publication is available at Springer via . <http://dx.doi.org/10.1007/s00603-014-0579-8>

**A note on versions:**

The version presented here may differ from the published version or, version of record, if you wish to cite this item you are advised to consult the publisher's version. Please see the 'permanent WRAP url' above for details on accessing the published version and note that access may require a subscription.

For more information, please contact the WRAP Team at: [publications@warwick.ac.uk](mailto:publications@warwick.ac.uk)



<http://wrap.warwick.ac.uk>

# Designing tunnel support in jointed rock masses via the DEM

C.W. Boon<sup>a</sup>, G.T. Houlsby<sup>a</sup> and S. Utili<sup>b</sup>

<sup>a</sup> Department of Engineering Science, University of Oxford,

Parks Road, Oxford OX1 3PJ, United Kingdom

<sup>b</sup> School of Engineering, University of Warwick,

Library Road, Coventry CV4 7AL, United Kingdom

Email: s.utili@warwick.ac.uk

Tel: +44 (0)24 765 22339, Fax: +44 (0)24 76418922

## Abstract

A systematic approach of using the distinct element method (DEM) to provide useful insights for tunnel support in moderately jointed rock masses is illustrated. This is preceded by a systematic study of common failure patterns for unsupported openings in a rock mass intersected by three independent sets of joints. The results of our simulations show that a qualitative description of the failure patterns using specific descriptors is unattainable.

Then, it is shown that DEM analyses can be employed in the preliminary design phase of tunnel supports to determine the main parameters of a support consisting of rock bolts or one lining or a combination of both. A comprehensive parametric analysis investigating the effect of bolt bonded length, bolt spacing, bolt length, bolt pretension, bolt stiffness and lining thickness on the tunnel convergence is illustrated.

The highlight of the proposed approach of preliminary support design is the use of a rock bolt and lining interaction diagram to evaluate the relative effectiveness of rock bolts and lining thickness in the design of the tunnel support. The concept of interaction diagram can be used to assist the engineer in making preliminary design decisions given a target maximum allowable convergence.

Also DEM simulations were validated against available elastic solutions. To the authors' knowledge, this is the first verification of DEM calculations for supported openings against elastic solutions.

The methodologies presented in this article are illustrated through 2-D plane strain analyses for the preliminary design stage. More rigorous analyses incorporating 3-D effects have not been attempted in this article because the longitudinal displacement profile is highly sensitive to the joint orientations with respect to the tunnel axis, and cannot be established accurately in 2-D. The methodologies and concepts discussed in this article, however, have the potential to be extended to 3-D analyses.

## Highlights

- a systematic approach of using the DEM as a design tool for tunnel support is demonstrated
- the concept of an interaction diagram of rock bolt spacing against lining thickness is illustrated
- methods to verify DEM calculations against available analytical solutions are provided
- a systematic analysis of the failure mechanisms occurring for unsupported tunnels for 3 joint sets is run

**Keywords:** tunnelling; rock bolt; lining; support; discrete element method; cavity expansion; interaction diagram

---

## NOTATION

$a$	Radius of tunnel opening
$A_b$	Cross sectional area of bolt
$D$	Diameter of tunnel opening
$d_{\text{bolt}}$	Bolt diameter
$d_{\text{init}}$	Initial active length of a bolt at a reinforced rock joint
$E$	Young's modulus of rock mass
$E_b$	Young's modulus of bolt

$E_L$	Young's modulus of lining
$F$	Bolt axial forces
$G$	Shear modulus of rock mass
$k_n$	Rock joint normal stiffness
$k_s$	Rock joint shear stiffness
$K_a$	Bolt axial stiffness
$K_L$	Rock-lining interface stiffness
$L_b$	Characteristic distance between adjacent reinforced rock joint
$n_b$	Number of bolts uniformly distributed around tunnel circumference
$M$	Bending moment in lining
$N$	Axial force in lining
$p_0$	Ground pressure at tunnel centre
$\Delta p$	Support pressure on the opening
$s_l$	Bolt spacing along tunnel axis
$s_\theta$	Bolt spacing along circumferential direction (unit: m)
$s_{\text{mean}}$	Mean rock joint spacing
$t$	Lining thickness
$\Delta r$	Convergence of tunnel lining
$\Delta u_{\text{ground}}$	Ground displacements
$\Delta u_{\text{lining}}$	Displacements of tunnel lining
$\Delta u_{\text{node}}$	Overlap distance between tunnel lining and ground
$\nu$	Poisson's ratio of rock
$\alpha, \beta$	Dimensionless variable for tunnel support
$\varepsilon_{\theta\theta}$	Strains along tangential direction

47

## 48 **1. Introduction**

49 The distinct element method (DEM) is rapidly gaining in popularity for the analysis of the behaviour  
50 of tunnels excavated in jointed rock masses (Vardakos et al., 2007). However, until now the method  
51 has not been used as a design tool but merely to verify the structural soundness of tunnel support  
52 systems (e.g. concrete lining, rock bolts, steel sets) designed via traditional empirical or analytical  
53 methods where the jointed rock mass is treated as a continuum and its mechanical properties are  
54 characterised according to classification systems (e.g. the Q-system (Barton et al. 1974), the Rock

Mass Rating (RMR) (Bieniawski 1983)) which consider the influence of joints via a smear approach disregarding single joints. Hence, the benefit of using numerical methods like the DEM for the design practice has been marginal (Barla et al. 2013). This article showcases a systematic approach where the DEM is employed in an active role in the design of tunnels in moderately jointed rock masses by means of which the main design parameters of supports made of either rock bolts or a lining only, or of a combination of both can be determined.

In a rock tunnelling project, the engineer is normally tasked to design support systems as economically as possible while still complying with a prescribed safety margin. In fact, the design must prevent any rock blocks from loosening and falling into the tunnel. The main support measures employed for jointed rock masses are rock bolts and lining (Hoek et al. 1995). The choice and extent of support depends largely on the failure mechanism. In most cases, it is helpful to anticipate the failure pattern of the unsupported opening so that effective support measures can be undertaken. For jointed rock masses intersected by discontinuities, the design philosophy is different between sparsely and moderately jointed rock masses (Hoek et al. 1995). For underground excavations in sparsely jointed rock masses with large joint spacing, stability is governed by key blocks whose shapes permit free kinematic movement into the opening. Failure involves either sliding or falling of key blocks. The study of key blocks has led to established analytical design procedures using stereographic projection techniques and block theory (Londe 1970; Goodman & Shi 1985; Goodman 1995). The engineer can identify key blocks from rock joint surveys, and secure them using pre-tensioned bolts.

However, designs based on key blocks are not suitable for underground excavations in moderately to heavily jointed rock masses. Sliding of large wedge structures is not normally encountered, as maintained by Bawden (1993) and Hoek et al. (1995). In contrast, failure usually involves ravelling or loosening of rock mass material into the excavation opening. This failure mechanism occurs in rock slopes as well (Utili and Crosta, 2011a, b). The failed material usually consists of numerous rock blocks. The complexity of the problem has led rock engineers to develop,

for the purpose of routine design, rock mass classifications based on past field data, such as the Rock Mass Rating (RMR) (Bieniawski 1983) and the Q-system (Barton et al. 1974). At present, depending on the cost and the importance of the project, the distinct element method is used to verify the support measures recommended by the rock mass classification systems. In this article, we explore the capability of the DEM to help engineers to design the support system since the initial phase of the support design for rock masses with complex joint patterns.

Finally, as the DEM is becoming more widespread, methods to audit numerical calculations deserve urgent attention (Hudson & Feng 2010). At present, confidence in the obtained results is largely drawn from past case-histories on which the DEM had been applied successfully (e.g. Barton et al. (1994), Bhasin et al. (1996), Vardakos et al. (2007)), rather than through thoughtful consideration of the actual engineering problem. Another objective of this paper is to provide a methodology for the validation of DEM simulations in order to increase the confidence of tunnel engineers in use of the DEM as a numerical tool for the prediction of the tunnel behaviour.

## **2. DEM analyses of unsupported openings**

In previous published studies of failure patterns of jointed rock masses, most investigators, e.g. Yeung & Leong (1997), Solak & Schubert (2004) and Solak (2009) modelled only two joint sets. In their results, the failure patterns showed limited variability, implying that support could be designed more efficiently, for instance more support could be installed at regions which are known to be more prone to failure. This research, however, is worth pursuing only if the trends obtained for two joint sets also hold true for jointed rock masses with more than two joint sets, as is the case with most jointed rocks encountered in civil engineering projects, e.g. Norwegian Olympic Ice Hockey Cavern at Gjøvik (Barton et al. 1994); The Shimizu Tunnel No. 3 located in Shimizu City (Vardakos et al., 2007); Gotthard highway tunnel (Zangerl et al. 2008); Lötschberg Base Tunnel (Deliso et al. 2013).

### **2.1 Numerical analyses**

In this exercise, complex jointed rock masses consisting of three independent sets of joints were modelled. Rock excavations with shallow cover depths ranging from 15 to 50 m have been reported in Dahlø & Nilsen (1994), Barton et al. (1994), Sjöberg et al. (2006) and Aksoy et al. (2010). The tunnels and caverns of the on-going East Side Access megaproject under the Grand Central Terminal in New York are approximately 50 m below ground level (Metropolitan Transport Authority 2013). Therefore, the opening diameter and cover depth employed in the simulations were 10 m and 50 m respectively to represent typical values found in the tunnel practice. A plot of the numerical domain is shown in Fig. 1.

All the 2-D simulations herein presented were run using the 3-D DEM code YADE (Kozicki & Donzé, 2008; Šmilauer 2010) by restricting the degrees of freedom of the rock blocks in the-out-of-plane direction, so that the blocks were allowed to translate in the  $y$ - $z$  plane only, and to rotate about the  $x$ -axis only. The algorithms employed for contact detection (see Boon et al. (2012) and Boon et al. (2013) for details) and the algorithm used for block generation (see Boon et al. (2014) for details) are based on a new conceptual framework which makes use of convex optimisation and linear programming (Boon 2013). The algorithm employed for block generation is capable of generating non-persistent rock joints so that block interlocking can be modelled. In the simulations here performed, we assumed that the discontinuities completely slice through any block that they reach, i.e. non-persistent discontinuities inside any intact block were assumed to develop fully such that the block is completely sliced. The rock blocks are assumed rigid. The contact law adopted for the rock joints is linearly elastic in the normal direction and linearly elastic perfectly plastic in the shear direction. After the rock blocks were generated, the in-situ stresses were initialized: i.e. gravity and horizontal forces were applied onto the horizontal “boundary blocks” of the domain of analysis. Hydrostatic in situ stresses were assumed ( $K_0 = \sigma_V / \sigma_H = 1$ ). Some damping was employed to accelerate the convergence of the rock mass under the initial loading to static equilibrium. During this generation stage, the same value of friction angle was assigned to all the joints, with the value being equal to the minimum friction required for the stability of the rock

blocks. This value was derived based on the weakest joint: given the in-situ  $K_0$  value, a stress circle in the Mohr plane is drawn for every joint orientation, and the highest friction angle among them is selected (Jaeger et al. 2007). This ensures that the generated stresses are homogeneous within the domain. Then, the blocks in the excavation opening were removed and support was installed simultaneously. Note that the boundaries in the horizontal direction and at the base of the model were as far as 30 m from the opening (see Fig. 1). Stress measurements at the boundaries after excavation were found to be minimally affected.

Table 1 provides a list summarising the failure patterns obtained for different joint orientations and joint friction angles. A total of 24 analyses were run. Our results for rock masses with three joint sets show that, by comparison to the case with two joint sets only (Yeung & Leong 1997; Solak & Schubert 2004; Solak 2009), there is a significantly larger degree of freedom with which the rock blocks can move into the excavated openings, and more than one failure pattern may occur.

Fig. 2 (a) shows the loosening of rock material at the roof. This is the more typical case of opening failure based on the experience from mining operations. For instance, in the Stability Graph Method (Potvin 1988), an empirical method used for cable-bolt design, susceptibility of openings to roof falls has been rated based on gravity-induced effects and joint inclinations. However, for certain joint patterns, stability of the sidewall may be more critical than the roof. Fig. 2 (b) shows the loosening of material at the sidewall. From all the cases simulated, it emerges that none of the rock masses failed uniformly around the opening and a certain degree of anisotropy is present. Hence, we can conclude that it is important that in the design phase the engineer does not make assumptions with regard to specific failure patterns. As gathered from field observations by Mathews et al. (1981), Potvin (1988), Potvin & Milne (1992) and Nickson (1992) for the Stability Graph Method for cablebolt design, joints with steeper inclinations are more prone to failure. The results of our simulations show that i) failure does not always occur along the steepest joint set (compare Fig. 2 (c) and (d)), which could be considered as counterintuitive; ii) nor does failure occur



along just any particular two joint sets; iii) it is possible for all the joint sets to participate in the failure mechanism (see the outline of the falling material in Fig. 2 (e)).

## **2.2 Conclusions**

From our analysis, it emerges that qualitative characterisation of the failure patterns using specific descriptions is unattainable. Let us consider for instance the roof failure in Fig. 2 (c). It is arguable that the failed material is bounded by joint sets which subtend the largest acute relative angle; at the same time, it is reasonable also to claim that the failed material is sliding along the steepest joint set. Hence, for practical purposes, the qualitative description of failure patterns (e.g. Table 1) should not be taken too rigidly. A pedantic approach towards the qualitative study of failure patterns is unhelpful and can be misleading.

Another crucial observation in this exercise is that, for the majority of joint patterns, more than one failure pattern took place at the same time. Concurrent failure patterns can be roughly categorized into three types. In the first case, two failure patterns occurred simultaneously and to approximately the same extent: for example, roof fall and sidewall failure (see Fig. 2 (f)). In the second case, the behaviour of the unsupported opening was dominated by one failure pattern only, while other minor gravity-induced rock fall were present (see Fig. 2 (g)). In the third case, initial falling or sliding of material led to more complex failure mechanisms. For instance, in Fig. 2 (h), the boundaries of the roof fall can be identified by a wedge shape; in this simulation, as the roof wedge slid off, the roof began to collapse from both sides of the wedge. In Fig. 2 (i), the failure mode evolved into a toppling mechanism, with material caving-in into the opening. When the orientations of two of the three joint sets were kept fixed, and the third set was varied, it was found that one of the failure patterns is affected (compare between Fig. 2 (j) and Fig. 2 (k)); roof failure had taken place in Fig. 2 (j), whereas sidewall failure had taken place in Fig. 2 (k). The great differences observed in terms of failure patterns highlight the importance of accounting for the realistic joint geometry of the rock mass in the design phase. Hence, from this set of analyses it emerges that a

parametric analysis of tunnel support systems based on two joint sets only would not be realistic because it gives rise to an oversimplified picture of the failure patterns. Rather, the actual number of joint sets has to be included in the engineering analysis. This is an important conclusion that practitioners need to include in their design practice.

As already mentioned in Section 2, spot bolting is normally used to support openings in sparsely jointed rock mass (Goodman, 1989), whereas systematic bolting is used in densely jointed rock mass (Barton et al. 1974; Bieniawski 1983). In light of our results, it emerges that also for moderately jointed rock mass with more than two joint sets, it is necessary to use systematic bolting because of the sensitivity of the failure mechanisms to the joint patterns. So our results highlight the need for the use of systematic bolting in the construction of tunnels in jointed rock masses (Carranza Torres, 2009). Systematic bolting is nowadays a key component of tunnel construction methods such as the New Austrian Tunneling Method (Rabcewicz 1964; Brown 1981).

### **3. Numerical implementation of support structures**

Subroutines have been specifically written by the authors to model the support structures considered, rock bolts and lining, in the open source DEM code YADE (Kozicki & Donzé 2008; Šmilauer 2010). These subroutines are called before the motion integration of blocks every time step (see Fig.3). At any given time step in a DEM calculation, blocks occupy a certain position in space, from which contact forces between overlapping blocks are calculated. In a similar manner, based on the positions of the rock blocks at the current time step, the forces resulting from block-support interactions are calculated from knowledge of their relative positions. Then, inertial forces on every block are calculated from the contact and support forces acting on each block, so that positions and velocities of the blocks can be updated.

#### **3.1 Modelling of the rock bolts**

There exist several rock bolt algorithms in the literature for discontinuum modelling. For every pair of mating rock blocks through which the rock bolt intersects at the time of installation, a spring is used to account for the restraint afforded by the bolt. A spring consists of a pair of anchor points, each of which is assigned to opposite mating rock blocks. An anchor point is fixed in the local reference frame of the rock block (to which it is referenced), so that it follows the motion of the reference rock block in global coordinates (see Fig. 4). The tensile force acting on the bolt is calculated from the elongations between the pair of adjoining anchor points.

The algorithm proposed by Lorig (1985) has been widely employed in DEM modelling since it was implemented into the commercial code UDEC (Itasca, 2004). The model accounts for both axial and shear resistances at the bolts via two springs located at the discontinuity interfaces; the first spring is oriented along the bolt axis to model the axial resistance of the bolts, while the second spring is perpendicular to this axis to model the shear resistance contributed by the bolts. The anchor points are located one to two diameters away from the discontinuity interface into each of the mating rock blocks (see for example Fig. 4 (a), although the figure shows only axial springs).

Other algorithms proposed for discontinuum modelling assume that the restraint afforded by a bolt is predominantly resisted by its axial forces, whereas its shear resistance is ignored. Since the axial direction of the rock bolt changes locally with the relative displacements of the two mating rock blocks, the direction of the axial force in most cases gives rise to resistance to shear motion as well (see Fig. 4). In this regard, Garga & Wang (1993) proposed to assign an anchor point midway between the two end points in a rock block through which the rock bolt passes (see Fig. 4 (b)). This is similar to the algorithms used in Shi (1988) and Kim et al. (1999), in that the anchor points are not intentionally placed close to the joints. Note that if the anchor points are assigned at the intersection between the rock bolt and the rock joints as was proposed by Moosavi & Grayeli (2006) (see Fig. 4 (c)), the axial force of the rock bolt is directed along the mating joint for the case of pure shear displacements. In terms of bolt contribution to the shear resistance of the reinforced rock joint, this choice can model only the “cohesion” effect parallel to the rock joint and not the

“confining” effect normal to the rock joint, according to the terminology used in Pellet & Egger (1996). To capture both the “cohesion” and “confining” effects, either the models in Lorig (1985) or Garga & Wang (1993) have to be used. In our analyses, in order to investigate the sensitivity of the bolt forces to the choice of the location of the anchor points, we ran two types of simulations with the anchor points located either midway between the rock joints (see Fig. 4 (a)) or 1.2 diameters away from the rock joints (see Fig. 4 (b)). Results are presented in Section 5.

Since one of the purposes of this paper is to showcase the use of DEM as a tool in the preliminary phase of tunnel design, it is important to keep the number of variables at a minimum; therefore, the rock bolt model consists of an axial spring only, i.e. the axial resistance of the bolt is considered to be dominant over the shear resistance of the bolts that can be neglected. Moreover, the inclusion of the shear spring would require the determination of a suitable value for the bolt shear stiffness which in turn requires further assumptions on other variables of uncertain determination such as the Young’s modulus of the grout material and the hole diameter for the grout. Furthermore, ignoring the shear component is a conservative assumption since larger displacements of the rock blocks are obtained. Finally, in the analytical solution of Pellet & Egger (1996) it is highlighted that, after the onset of plastic hinges in the bolts (anchor points in our numerical model), the bolt segment crossing a rock joint can be considered, from a structural viewpoint, equivalent to a truss subject to an increasing axial force and a constant shear one. In this respect, it is worthy to note that the bolt shear resistance is commonly neglected in the finite element modelling of rock bolt support, based on the assumption that the displacements are fairly uniform around the opening. For instance, in Liu et al. (2009), Bobet (2009) and Bobet & Einstein (2011) bolts are modelled as truss elements able to resist tensile or compressive forces only.

In our DEM simulations, rock bolts were simulated by applying a force to every pair of rock blocks making up the bolted rock joint. The force,  $\mathbf{f}$ , is applied at the anchor points,  $\mathbf{p}_1$  and  $\mathbf{p}_2$  (Fig. 4 (a)), and is oriented along the direction which connects them. The magnitude of the force,  $\mathbf{f}$ , is based on their elongation:

$$\hat{\mathbf{f}} = \frac{(\mathbf{p}_2 - \mathbf{p}_1)}{\|\mathbf{p}_2 - \mathbf{p}_1\|} \quad (1)$$

$$\mathbf{f} = K_a (\|\mathbf{p}_2 - \mathbf{p}_1\| - d_{init}) \hat{\mathbf{f}} \quad (2)$$

where  $d_{init}$  is the initial distance between  $\mathbf{p}_1$  and  $\mathbf{p}_2$ .

### 3.2 Modelling the lining

In the literature, different methods have been used in the DEM to model lining supports for an underground opening. A simple way to model the effect of lining support for a circular opening is to model the lining as a closed-chain of geometrical entities (e.g. circular particles), between which a strong bond exists to resist shear forces and moments (Funatsu et al. 2008) (see Fig. 5 (a)). However, in this method, the values for the bond stiffnesses are arbitrarily determined, i.e. their values cannot be related to the physical parameters characterising the support.

Alternatively, the physical relationship between adjoining geometrical entities can be modelled by a linear beam model so that the structural properties of the lining in terms of axial and bending stiffnesses can be inputted in the model directly (see Fig. 5 (b)). This beam algorithm has been employed by Makurat et al. (1990), Bhasin et al. (1996) and Chrysanthakis et al. (1997), and has also been implemented in the commercial code UDEC (Itasca 2004). The internal forces of the lining are calculated based on the displacements and rotations of the geometrical entities (Case & Chilver 1971). The geometrical entities are represented as nodes, i.e. circular DEM particles with zero radius but possessing a lumped mass. The forces acting at the lining-rock interface are modelled as contact forces between nodes and rock blocks.

The lining in this study was modelled as a series of nodal points around the excavation opening (see Fig. 5 (b)). Each nodal point was assigned a lumped mass. Fig. 6 shows how the contact forces between lining nodes and rock blocks can be derived from the depth of penetration of the nodes into the rock blocks. The contact forces on the nodes (or lumped masses) are calculated

in the same manner like any other DEM particle. These lumped masses were connected using linear beams which restrain the movement of the nodes due to the presence of the contact forces exchanged with the rock blocks (see Fig. 6). The method of approximating a non-linear geometrical shape through the interpolation of piecewise linear models is commonplace in engineering numerical analyses and provides accurate results, as long as the level of discretisation is sufficiently fine. In principle, more accuracy could be obtained using piecewise curved-beams. However, the error introduced from adopting linear beams is small compared to the idealisation of planar rock joints; in fact, natural rock joints are usually wavy and, depending on the geology, can be folded too. Because of the numerical artifice that a gap exists between nodes, the spacing between nodes was always kept smaller than the rock joint spacing. However, occasionally due to the way joints intersect in the proximity of the tunnel opening, there may be small rock blocks escaping between two adjacent nodes.

Since the support lining is designed to remain in the elastic regime, the beams were assumed to be elastic, so that standard calculation procedures for framed structures were used to work out the internal forces of each beam segment (Case & Chilver 1971).

#### **4. Design of the support system**

The numerical models were generated based on the procedures detailed in Section 2.1. The cover depth and opening diameter here were assumed to be 20 m and 10 m respectively. Support was installed immediately after excavation, i.e. wished in place. At the same time, the reference (initial) positions of the rock bolts and lining nodes were assigned. In order to validate the numerical analysis against closed-form solutions, the case of a tunnel subject to an isotropic stress field ( $\sigma_v = \sigma_h$ ), so that axisymmetric conditions apply, is herein considered. Further, the contribution to resistance from the tunnel face was assumed to be negligible.

An example case is herein provided to illustrate the use of the DEM as a design tool to model underground openings in jointed rock masses with support structures. The failure pattern for the

unsupported opening is shown in Fig. 7 (a). The study begins with a support consisting of rock bolts only (section 5), then of a lining (section 7), finally considering a composite support made of both a lining and rock bolts (section 8). The values adopted for the parameters in the numerical simulations are shown in Table 2. In practice, these values can be determined experimentally or from field surveys.

## **5 Results for a support made of rock bolts only**

### **5.1 Validation of DEM simulations with rock bolt support against analytical elastic solution**

In this section, the DEM calculations with rock bolt support are validated against the elastic solution proposed by Carranza-Torres (2009) for a circular opening in a rock mass subjected to isotropic stresses. In Carranza-Torres (2009), the axial stresses of the bolts are assumed to be smeared into the rock mass uniformly in both the circumferential and longitudinal directions. The elastic constitutive equations for both rock bolts and rock, together with the equilibrium equation expressed in terms of radial and circumferential stresses, can be rearranged into a single differential equation expressed in terms of a single unknown: the radial displacements. For sake of completeness, there is another analytical approach by means of which the rock bolt stresses could be estimated known as the shear-lag method in which the equations of equilibrium are derived for a single rock bolt (Li & Stillborg 1999; Bobet 2009). This method, however, has several shortcomings which have been discussed in detail by Bobet & Einstein (2011). This method is not used in this validation exercise mainly because (i) the interaction between adjacent bolts is disregarded in its derivation and (ii) the calculation requires as input the shear resistance at the interface between the rock bolt and rock mass; but the shear force acting along the bolt interface is often not known *a-priori*, whereas the axial stiffness can be determined from pull-out tests as illustrated in Stillborg (1994).

As shown in Carranza-Torres (2009), assuming that the opening is wished-in-place (i.e. lining installed immediately after excavation) and that the rock bolts are installed without pretension, the

relative stiffness of the ground-structure can be characterised by the following dimensionless variable,  $\beta$ :

$$\beta = \left( \frac{1}{s_{\theta}s_l} \right) \frac{K_a s_{\text{mean}}}{2G} \quad (3)$$

where  $s_{\theta}$  (units: m) and  $s_l$  (units: m) are the rock bolt spacing in the circumferential and longitudinal directions measured along the tunnel perimeter, and  $s_{\text{mean}}$  is the mean joint spacing which is characteristic of the rock mass. Rock bolt radial stresses and convergence can be calculated from the general solution of the differential equation derived by (Carranza-Torres 2009) imposing the appropriate boundary conditions.

A closed-form analytical solution was derived in Carranza-Torres (2009) for the case of continuous, homogeneous and isotropic rock. To employ the solution on a heterogeneous jointed rock mass, first an equivalent shear modulus,  $G$ , of the jointed medium has to be calculated (see Eq. (3)). There are several ways by which the elastic constants of a jointed rock mass can be estimated. A recent review of the analytical and empirical solutions proposed in the literature can be found in Zhang (2010). The method illustrated in Goodman (1989) is used here as a first estimate, since this method (Duncan & Goodman, 1968; Kulhawy 1978) is conceptually straightforward and could be used as a benchmark for other methods. In Goodman (1989), considering a jointed rock mass with uniform joint spacing  $s_{\text{mean}}$ , its equivalent elastic modulus  $E$  is approximated as:

$$\frac{1}{E} = \frac{1}{E_i} + \frac{1}{k_n s_{\text{mean}}} \quad (4)$$

with  $k_n$  being the rock joint normal stiffness, whilst its equivalent shear modulus  $G$  can be approximated as:

$$\frac{1}{G} = \frac{1}{G_i} + \frac{1}{k_s s_{\text{mean}}} \quad (5)$$



with  $k_s$  being the joint shear stiffnesses, where  $E_i$  and  $G_i$  are the elastic modulus and shear modulus of the intact rock material respectively. Since rock blocks are rigid in our DEM simulations, the equivalent Young's modulus,  $E$ , reduces to:

$$E = k_n s_{\text{mean}} \quad (6)$$

whilst the equivalent shear modulus,  $G$ , to:

$$G = k_s s_{\text{mean}} \quad (7)$$

Eq. (7) is used in the method of estimation denoted as G1 in Table 3. Although the Poisson's ratio,  $\nu$ , is not necessary to determine the equivalent  $G$ , an assumption on its value is still required in the analytical solution derived by Carranza-Torres (2009). A Poisson's ratio of 0.2 was here assumed. Alternatively, the equivalent shear modulus can be calculated from the equivalent Young's modulus based on elasticity theory:

$$G = \frac{E}{2(1 + \nu)} \quad (8)$$

Substituting Eq. (6) into Eq. (8), we obtain:

$$G = \frac{k_n s_{\text{mean}}}{2(1 + \nu)} \quad (9)$$

This method for the estimation of the shear modulus (Eq. (9)) is denoted as G2 (see Table 3).

A simple although approximate method to calculate the mean joint spacing,  $s_{\text{mean}}$ , is to draw a straight line and divide its length by the number of times it intersects the rock joints. This method is analogous to measuring the total number of discontinuities in a scanline, from which the mean spacing can be calculated from its inverse (Priest & Hudson 1976). Based on this procedure, the mean spacings along three radial directions were calculated (0.77 m, 0.83 m, 0.714 m). A mean spacing of 0.77 m corresponding to the average of the three calculated values was adopted.

The aforementioned approaches of approximating the elastic and shear moduli are strictly speaking valid only for regular joint patterns. Since the joint patterns here considered are far from regular (three independent sets of random joints), it is evidently desirable to have a second

alternative method to determine the elastic properties of the jointed rock mass. To this end, the authors performed a numerical 1-D compression (oedometric conditions) on the model domain employed in the DEM simulations. In this test, a vertical stress  $p_0 = 662 \text{ kPa}$ , equal to the stress value present at the tunnel centre, was applied on the top boundary of the domain with the lateral boundaries of the domain restrained in the horizontal direction. Unlike actual laboratory oedometer tests, the horizontal stresses acting on the lateral boundaries can be easily measured in DEM simulations, making the determination of the elastic constants possible. Assuming that the material is isotropic, from Hooke's law we derive:

$$\sigma_1 = (\lambda + 2G)\varepsilon_1 + \lambda\varepsilon_3 \quad (10)$$

$$\sigma_3 = \lambda\varepsilon_1 + (\lambda + 2G)\varepsilon_3 \quad (11)$$

where  $\lambda$  is the Lamé's constant. Substituting  $\varepsilon_3 = 0$  in Eqs. (10) and (11), we obtain:

$$G = \frac{(\sigma_1 - \sigma_3)}{2\varepsilon_1} \quad (12)$$

from which the elastic shear modulus can be calculated. This third approach is denoted as G3 in Table 3. The deformability approximated through these models could also be verified with in-situ measurements routinely carried out in practice, such as the plate jacking test, the Goodman test and the plate loading test (Palmström & Singh, 2001), or through classification systems such as the Geological Strength Index (Cai et al., 2004; Hoek & Diederichs, 2006).

The values of the shear moduli estimated via the three employed approaches are summarised in Table 3. It emerges that the shear moduli estimated via approaches G1 and G2 differ by approximately 4 times. There are two possible reasons for this discrepancy. First, these methods were derived assuming ideal regular joint patterns so that when they are applied to random joint patterns, discrepancies between the two are likely to arise. Second, the normal to shear stiffness ratio,  $k_n/k_s$ , is a parameter subject to great variability depending on the rock type with scanty experimental data available. Bandis et al. (1983) run tests on five different types of rocks concluding

that the  $k_n/k_s$  ratio of a rock joint varies with the level of normal stresses applied; however for normal stresses greater than 0.2 MPa, the ratio can be well approximated by a constant value equal to 10. Therefore, we adopted this value which is also consistent with the values adopted in several other DEM simulations of jointed rock masses (Shen & Barton 1997; Eberhardt et al. 2004; Jiang et al. 2006; Hammah et al. 2008). It is reassuring that the shear modulus, estimated using Eq. (12) via DEM simulations, falls between the values estimated by Eqs. (7) and (9).

Other 1D compression tests were under different conditions to check the sensitivity of the value of  $G$  determined via DEM simulations to the value of the friction angle adopted for the joints, the size of the domain of simulation and the direction of compression. In case a higher rock joint friction angle is assigned (G4 approach in Table 3), the effect on the determination of  $G$  is found to be marginal. This indicates that at the level of stress considered, the amount of irreversible (plastic) sliding between rock blocks is very small in comparison with the elastic displacements. With regard to the domain size, Ivars et al. (2011) showed that scale effects may be important; hence we ran 1D compression tests on different domain sizes. However, as in Staub et al. (2002), similar deformability properties were obtained for the different sizes of the sampling domain that were investigated (G5 and G6 in Table 3). 1D compression tests were also conducted along the horizontal direction (G7 and G8 in Table 3). In this case, the  $G$  values were found to be slightly higher than those obtained from vertical compression. Given the fact that the difference is small, it can be stated that the elastic properties of the DEM domain are fairly isotropic.

In Fig. 8 (a) – (c) the values of the axial bolt forces obtained from the DEM simulations of three different configurations of bolt reinforcement are plotted against the distance from the tunnel axis (see the symbols in the figures). The bolt forces are normalised by the ground pressure at the tunnel centre,  $p_0$ , and the tunnel diameter,  $D$  (refer to Fig. 1 again for notation). The bolt configurations of the DEM simulations are shown in Fig. 9. In Fig. 8 (a) – (c), also the bolt forces predicted by the analytical elastic solution of Carranza-Torres (2009) for the values of shear moduli determined from the three approaches employed (G1; G2; G3; see Table 3) are plotted as

continuous lines. The calculation of the bolt forces from the closed-form equations of Carranza-Torres (2009) is illustrated in Appendix A. Some scatter between the analytical predictions and the DEM results is to be expected given the highly irregular joint patterns of the rock mass. In case of small spacing between rock bolts ( $11.25^\circ$ ), the DEM results compare fairly well with the elastic solution. However, the discrepancy increases for larger spacings ( $15^\circ$  and  $22.5^\circ$ ).

Note that the closed-form solution in Carranza-Torres (2009) assumes that the material is homogeneous and elastic, the bolts are evenly distributed around the opening, the stresses are isotropic and the presence of gravity is ignored. On the contrary, in the DEM models, the material is heterogeneous and inelastic, bolts are not installed at the invert of the opening, stresses are not isotropic, and gravity is present. Therefore, the good agreement obtained for small bolt spacing ( $11.25^\circ$ ) is very encouraging. In fact, the trend that the discrepancy increases as bolt spacing increases ( $11.25^\circ$ ,  $15^\circ$  and  $22.5^\circ$ ) is also consistent with well-known analytical solutions developed based on the convergence confinement method (Brown et al. 1983, Carranza-Torres & Fairhurst 1999). According to the convergence confinement method, when the support pressure is below a critical value, the material around the opening becomes plastic. The thickness of this plastic zone increases as the support pressure is reduced. To put it another way, as the bolt spacing increases, the rock mass around the opening begins to exhibit plastic behaviour, so that the discrepancy with elastic solutions is expected to increase.

## **5.2 Influence of bolt bonded length, spacing, length and pretension**

In the design of rock bolts, length and spacing are the chief parameters of concern, because they are directly related to the cost of support. This section shows how the length and spacing of the rock bolts can be determined using the DEM not just as a verification tool to be employed after the design phase but as a proper design tool.

A particular rock bolt specification has to be considered as the starting point for the iterative design procedure hereafter illustrated. From Stillborg (1994), for a 20-mm-diameter steel bar with

ultimate tensile strength of 180 kN, the axial stiffness obtained by pulling two blocks of concrete apart is approximately 0.1 GN/m. This test is more representative of field conditions for a rock mass intersected with discontinuities. In this exercise, a more conservative bolt specification of harmonic steel was used as a first case, i.e. 28 mm, and the axial stiffness was assumed to correspond approximately to 0.2 GN/m. In practice, this value is provided by the bolt manufacturer. Some bolt suppliers may specify only the grade and Young's modulus of the steel. But for a jointed rock mass, the axial stiffness of a bolt across a rock joint is the most important parameter. As a starting point, a dense support system was modelled, i.e. long rock bolts with small spacing (see Fig. 7 (b)). This configuration, consisting of 21 bolts each 7 m long with spacing of  $11.25^\circ$  around the crown and springing, was chosen as reference configuration.

First the influence of the length of bonding of the bolts was investigated. Two values of bonded length were considered. In the first one, the bolt anchor points are placed 1.2 bolt diameters away from each joint (see Fig. 4 (a)) as in Lorig (1985). In the second one, the anchor points are placed midway between the two points at which the rock bolt intersects the rock block (see Fig. 4 (b)) as in Garga and Wang (1993). In Fig. 10 (a) and (b) the results of the two numerical implementations are compared in terms of maximum normalised bolt forces and displacements for the reference bolt configuration (see Fig. 7 (b)). From the figures, the results calculated for the two values of bonded length are very close – the largest percentage difference being 8.1 % and 4.0% for bolt forces and displacements respectively. In all the analyses presented hereafter, the anchor points were placed close to the joints, i.e. with an offset distance of 1.2 diameters away from each joint (see Fig. 4(a)).

In Fig. 11, the distribution of the axial force acting in each rock bolt normalised by the maximum value of force is plotted against the distance from the tunnel centre for the reference configuration (7 m long with spacing of  $11.25^\circ$ ). Fig. 11 and Fig. 9 (a) show that most of the forces follow a common pattern: all the curves reach a peak and then tail off away from the excavation opening. Also it can be noted that the bolt forces are roughly constant beyond 1.8 times the tunnel

radius (4 m) from the tunnel centre (see Fig. 11). Moreover, significant scatter of bolt forces can be observed. The most obvious source of scatter is because the rock joints are non-uniform, and the geometrical properties of the rock joints (i.e. spacing, orientation and extent) follow probabilistic distributions.

In the second configuration (see Fig. 9 (b)), 4 m long bolts were considered and the bolts below the springing of the opening were removed. A parametric analysis for increasing bolt spacing was then conducted with spacing of  $15^\circ$  and  $22.25^\circ$  (see Fig. 9 (c) and Fig. 9 (d)). From the results it emerges that bolt forces and displacements increase marginally when the spacing is increased from  $11.25^\circ$  to  $15^\circ$  (see Fig. 12 (a) and (b)). Instead, when the spacing is increased from  $15^\circ$  to  $22.25^\circ$ , bolt forces and displacements increase significantly. Also significant ravelling of rock blocks occurs between the bolts (as shown previously in Fig. 9 (d)), indicating that a bolt spacing of  $22.5^\circ$  or greater would be unsafe. In Fig. 13 the trend of bolt forces and displacements at the crown versus bolt spacing is plotted.

An interesting observation is that the maximum bolt forces,  $F$ , when normalised by the product of characteristic pressure,  $p_0$ , and bolt spacing,  $a\vartheta_b$ , are roughly similar for different values of bolt spacing (see Fig. 14 (a)). The results indicate that the normalised forces ( $F/p_0D\vartheta_b$ ) decrease slightly as the bolt spacing increases. This trend was confirmed by repeating the analyses for different joint patterns (see Fig. 14 (b) and (c)). For the ideal case in which the rock bolts are uniformly distributed and the far-field stresses isotropic, the product of pressure and bolt spacing ( $p_0a\vartheta_b$ ) can be interpreted as the upper bound load per bolt.

Although pretension is not present in the rock bolt recommendations for rock mass classifications such as the RMR system (Bieniawski 1983) and the more recent version of Q-system (Barton 2002), it is common practice in several countries to introduce pretension in rock bolts (Liu et al., 2009). Therefore we examined the influence of pretension. Analyses were run for various values of pretension uniformly applied to all the bolts. From Fig. 15 (a) where the normalised radial convergence is plotted, it emerges that pretension is effective at reducing radial displacements. For

bolt pretension of 100 kN and 150 kN, the displacements around the opening is found to be more uniform; the differential displacements between the crown and the springing are smaller. Nevertheless, in terms of overall displacements, the influence of pretension is found to be minor. Also using pretension leads to an increase of bolt forces (see Fig. 15 (b)) which in turn may lead to the need for bolts with higher yield limits.

From the performed analyses, it can be concluded that 4 m long bolts placed at 15° spacing can be considered to be a suitable design configuration. In this particular example, it seems that pretension is not advantageous because of its limited benefit. To examine this conjecture, simulations were run for larger bolt spacing (22.5°), with either bolts of longer length or higher pretension applied. From Fig. 16 (a) it emerges that increasing the bolt length from 4 m to 7 m does not induce a significant change of displacements; from Fig. 16 (b) it emerges that although introducing pre-tension of 150 kN results in smaller displacements, the bolt forces increased substantially so that bolts with higher yield limits would have to be used. Moreover, the ravelling of rock blocks between bolts persists as shown in Fig. 17. Hence, it emerges that pretension is only effective at controlling displacements locally around the bolt. The results show that the use of a larger bolt spacing counterbalanced by longer bolt lengths or higher pretension is not an effective design measure.

## **6. A note on the variability of ground properties and rock bolt forces**

It is important to point out that the results of the previous analyses are unable to predict precisely the values of the actual bolt forces in the field, because a joint pattern generated numerically from a statistical input is analogous to a random sample. For a rock mass intersected by a large number of rock joints, the rock joints are characterised using probabilistic distributions for design purposes. This is in contrast to sparsely jointed rock masses where the exact spatial coordinates and orientations of the joints can sometimes be deterministically measured, in which case the most critical cross-section of the underground excavation is analysed in the numerical modelling. To put it

another way, a joint pattern generated from statistical input data is only one of the many possible engineering outcomes. To reduce the level of uncertainty in this calculation, the engineer can repeat the simulations using different “samples” generated from the same statistical input. Depending on the in-situ stress ratio, the number of joint sets and their relative spacing and extents, the assumption of an equivalent isotropic medium may be acceptable for engineering purposes, in which case one can fairly assume that the forces experienced in the bolts are independent and non-correlated, the data from the different numerical “samples” can be merged to increase the sample size, i.e. the number of calculated bolt forces. A large sample size can estimate the distribution of the “population” better and less scatter in the distribution of the calculated bolt forces can be expected.

A simple way to visualise scatter is via frequency histograms. In Fig. 18 the histograms of maximum bolt forces for three different “samples” of joint patterns are plotted. The data obtained from the three samples can be analysed using statistical tools as shown in Fig. 18 (d). Note that the fitting of statistical distributions was conducted on the raw data rather than on the histograms. In most situations, the distribution can be modelled as a normal distribution. In this example, the mean of the normalised maximum bolt forces is 0.03 and the standard deviation is 0.009.

Instead of merging the data, one can analyse the bolt forces from different simulations separately. One way is to calculate the confidence intervals for each statistical distribution. Alternatively, if a probability distribution is a function of a parameter  $\chi$ , this parameter can be treated as a random variable and updated recursively using techniques such as Bayesian estimations (Montgomery & Runger 2010). Bayesian estimation techniques can also take into account prior information of the ground obtained from previous projects where the local geology is similar.

## **7. Results for support made of lining only**

### **7.1 Comparison with elastic solution for an opening with lining support**



As in the case of rock bolt support, DEM simulations for a lining support are first validated against analytical solutions. The elastic solution employed for this purpose is taken from cavity expansion theory for an elastic medium, assuming that the opening is supported by a thin-walled cylinder (Crandall et al. 1978). Based on the theory for thin-walled cylinders, the axial forces in the lining can be calculated as (see Appendix B for derivation):

$$N = \frac{p_0 E_L t K_L a}{2K_L G a + \frac{2E_L t G}{a} + E_L t K_L} \quad (13)$$

where  $E_L$  is the elastic modulus of the lining,  $K_L$  is the stiffness at the rock-lining interface,  $t$  is the lining thickness,  $a$  is the opening radius,  $G$  is the ground shear modulus and  $p_0$  is the ground characteristic pressure. The three values of the equivalent shear modulus for the jointed rock mass calculated in section 5 (G1; G2; G3 in Table 3) were employed in the DEM simulations. Fig. 19 (a), (b) and (c) show the axial forces recorded in the DEM calculations at each lining beam element in comparison with the elastic solutions for three different values of the lining-rock interface stiffness, namely 1 MPa/m, 0.1 GPa/m and 1 GPa/m respectively.

The averaged values are plotted and compared for a wider range of interface stiffnesses in Fig. 20. The comparison is encouraging, in that the DEM solutions obtained for large values of the interface stiffness are bounded between the elastic solutions based on the estimated shear moduli (refer to Table 3). Instead, for low interface stiffnesses, the axial forces calculated by the DEM simulations are higher than the elastic solutions. This is reasonable because, in case of low interface stiffness, plastic displacements between rock blocks are likely to take place, thereby increasing the pressure on the lining. Note that Malmgren & Nordlund (2008) also observed using UDEC (Itasca 2004) that the lining axial force increases with the rock-lining interface strength.

## 7.2 Influence of bending stiffness

An understanding of the influence of the bending stiffness of the lining on the tunnel behaviour can help the engineer to design the lining cross-section. If reinforced concrete is used, an understanding

of the influence of bending stiffness also helps the engineer to evaluate the consequence of cracking which normally causes a reduction of the bending stiffness of the lining. The reduction of bending stiffness is also a simplified way to consider the influence of radial joints in segmented linings (Muir Wood 1975). Fig. 21 (b) shows that, for decreasing bending stiffness, the lining experiences smaller bending moments. Herein, bending moments which are sagging inward into the opening are taken as negative. The result that the support load is proportional to the support stiffness is consistent with common engineering knowledge. The same trend was obtained by Steiner & Meier (1996) for openings subjected to anisotropic in-situ stresses using the closed-form equations proposed by Einstein & Schwartz (1979) for tunnel design. From the DEM analyses shown in Fig. 21 (a), the axial forces were found to generally increase also with bending stiffness. This finding is logical because a higher bending stiffness will impose larger constraints on lining deformations. This finding also agrees with the analyses conducted by Son & Cording (2007) using UDEC (Itasca 2004) for an intact elastic rock mass.

## **8. Results for a composite support made of rock bolts and lining**

It is of great interest to the tunnel engineer to design tunnel support systems based on sound numerical modelling and engineering judgement. In general, a suitable support system should be designed so that the stresses within bolts and lining remain below the yield limit. The thicker is the lining, the lower the bolt forces and the smaller the convergence are expected (see Fig. 22 (a) and (b)). The axial forces and bending moments on the lining increase for increasing lining thicknesses (see Fig. 23 (a) and (b)). In this example, the benefit of introducing a 0.01D thick lining to an unlined opening is significant, reducing ground convergence by almost half (see Fig. 22 (b)). A subsequent increase in lining thickness reduces further the opening convergence, but to a lesser extent. From a cost-benefit viewpoint it looks like a 0.01D (10 cm) lining can be considered as favourable in this example, unless a smaller convergence is desired.

### **8.1 Interaction design diagram**

In general the optimal bolt configuration and lining thickness is a function of the desired target convergence. The design of support consisting of both rock bolts and lining is a rather complex problem, since there are two ways by which ground convergence can be controlled: either by the rock bolts or by the lining. The design procedure illustrated in section 7 attempts to find the optimal lining thickness, starting from a particular rock bolt configuration. Equally, it is also possible to start from an input lining thickness and work out the optimal rock bolt configuration. If either of the two procedures are repeated for different combinations of lining thickness and rock bolt spacing, the results are well summarised by an interaction diagram (see Fig. 24) where contours of tunnel convergence are plotted in the bolt spacing – lining thickness plane. The engineer can use this interaction diagram to make the optimal design decision given a target maximum allowable convergence. Also the diagram can help the engineer to gauge the effectiveness of introducing an “increment” of either rock bolt support or lining support. The choice for the optimal combination between lining and rock bolts depends on the cost of the two options which may vary over time and is a function of several factors such as the country where the tunnel is built and many site specific variables such as the cost of local labour, the cost of material haulage, etc. The interaction diagram plotted in Fig. 24 is meant to be used by the tunnel engineer as a technological design chart providing the possible combinations of rock bolt intensity and lining thickness (the locus of points on a contour line) to keep the convergence within a specified limit. The design chart accounts for the mechanical response of the tunnel for a variety of possible support systems but does not account for the associated costs. The choice among the possible combinations of input values giving rise to the same amount of convergence, i.e. the amount of rock bolt versus lining thickness, will be done by the engineer accounting for the costs required for rock bolt and lining installation. Since the costs are site specific, the choice will be site specific too.

In this paper, this technique is illustrated for the case in which the opening is wished-in-place, however the procedure can be repeated for any case where the support is installed at any time after excavation by adopting an appropriate fictitious support pressure accounting for the

effect of tunnel advancement (Wang et al., 2013b). The interaction diagram (Fig. 24) suggests that for lining thicknesses of 0.02D or greater, the contribution of rock bolts is marginal so that the ground convergence is mainly resisted by the lining. In this example, a good choice to ensure a balance in terms of the relative contributions of lining and bolts to preventing tunnel convergence is the adoption of a 0.01D (10cm) thick lining with 15° spacing between rock bolts. The annotations in red are the results obtained from using different bolt stiffnesses, and they are discussed in the next section. Note that similar diagrams could also be used to display the contour of other variables of interest, such as maximum bolt forces or lining stresses to verify they are below specified limits.

In principle, an interaction diagram can be generated for each block geometry (related to Sec 6). However to optimise the number of simulations, the desired rock support combination could be determined first for a particular block geometry. Then, for the most representative block geometry, a statistical approach to address block geometry sensitivity could be carried out as illustrated in Sec.6. But, if a more rigorous analysis is considered necessary, an interaction diagram can be obtained for every block geometry generated, which could be later consolidated together based on the mean.

Finally, in this paper, we do not consider the influence of creep on tunnel convergence which can be significant for certain types of squeezing rocks (see for instance Barla et al. 2012). However, there is no conceptual difficulty in including creep in DEM simulations by either prescribing time-dependent rheological laws to the rock blocks from experimentally determined constitutive laws (Barla & Debernardi 2009) or by calibrating time-dependent contact laws reflecting the time dependent rock behaviour observed at the meso-scale. In this way it is possible to produce interaction diagrams providing the value of tunnel convergence at various times and accounting for the effect of construction sequence (Wang et al., 2013a; Carranza Torres & Fairhurst, 2000). To relate the longitudinal displacement profile to 2-D, the engineer may approximate the traction loss or preconvergence in 2-D from a 3-D simulations (Carranza-Torres & Fairhurst, 2000; Vlachopoulos & Diederichs, 2009). Note that, for a jointed rock mass, it is necessary to run 3-D simulations to

establish the longitudinal displacement profile because the results are highly sensitive to the joint orientations with respect to the tunnel axis. If 3-D effects are modelled such as the influence of tunnel displacements before support installation and the influence of delayed support, an interaction diagram can be generated for each history of installation.

## **8.2 Influence of rock bolt stiffness**

Like any other composite structure, the load distribution between the materials depends on their relative stiffness. Therefore, if the stiffness for the rock bolts is reduced, the bolt forces will reduce correspondingly (see Fig. 25 (a)); and the loads (axial forces and bending moments) on the lining will in turn increase, as shown in Fig. 26 (a) and (b). In this example, the considered changes in bolt stiffness ( $\frac{1}{3} K_a$  and  $3K_a$ ) influence the tunnel convergence and lining loads only very slightly.

An estimate for changing the stiffness values can be obtained from the interaction diagram plotted in terms of dimensionless groups. Note that the dimensionless bolt axial stiffness depends on both bolt spacing and bolt stiffness, and it is possible that two different bolt configurations have the same dimensionless value. The results obtained for bolt stiffnesses of  $\frac{1}{3} K_a$  and  $3K_a$  are plotted in the interaction diagram (see Fig. 24) in red. It is important to warn that the final design should still be verified against a numerical simulation run for the design values of the support system because errors from extrapolating the optimal values for lining and rock bolt support from an interaction diagram built by performing a finite number of numerical simulations unavoidably can be significant, particularly when the ground convergence is sensitive to small variations of the support. This is the case in the regions of the diagram where a high gradient of the convergence contour lines exists (see Fig. 24).

## **8.3 Influence of in situ stresses**

Uncertainties on the ground data obtained from site investigation and/or geological variability can lead to significant discrepancies between the ground response predicted by the numerical model

and the one observed in situ. So it is useful to investigate by parametric analyses the influence that in-situ stresses can have on the rock bolts and lining respectively which is summarised in Fig. 27 and Fig. 28. When the horizontal-to-vertical stress ratio,  $K_0$ , is smaller than 1.0, the crown experiences larger displacements compared to the springing (Fig. 27 (b)). In contrast, for higher stress ratios, the springing experiences larger displacements. In this example it turns out that in case of anisotropic in-situ stresses, the bolt axial forces (Fig. 27 (a)) remain close to the values determined in the hydrostatic case. However, let us emphasise that this observation on the bolt forces is not universal and may be true only for the particular joint patterns here considered. For  $K_0 = 1.5$ , the crown and invert of the lining experience larger axial forces (see Fig. 28 (a)).

## 9. Conclusions

Several 2D DEM analyses were performed to identify the potential failure mechanisms occurring in the excavation of a circular unsupported tunnel in a rock mass intersected by three independent sets of joints. The results of our simulations show that i) failure does not always occur along the steepest joint set, which is rather counterintuitive; ii) nor does failure occur along just any particular two joint sets; iii) it is possible for all the joint sets to participate in the failure mechanism; iv) the failure mechanisms are numerous. Therefore, it emerges that the prediction of the exact failure location is unlikely to be successful in practice since the failure location is highly sensitive to the joint patterns and there could be more than one failure mechanism taking place at the same time. So a qualitative description of the failure patterns using specific descriptors is unattainable. Hence, the study underpins the conventional geotechnical practice of supporting a large circumference of the tunnel opening for moderately to heavily jointed rock masses.

It has been shown that DEM analyses can be employed in the design phase of tunnel supports in order to determine the main parameters of supports consisting of rock bolts, one lining or a combination of them. A comprehensive parametric analysis was run investigating the effect of bolt bonded length, bolt spacing, bolt length, bolt pretension, bolt stiffness, lining thickness on

tunnel convergence for different in-situ stresses. The use of numerical methods for the design of the tunnel support represents a significant step forward from traditional empirical or analytical methods which use rock mass classification systems (Barton et al., 1974; Bieniawski, 1983) to characterise the mechanical properties of the rock which is treated as a continuum and therefore cannot adequately capture the behaviour of the rock mass especially in cases where the geology deviates significantly from the dataset of site investigations employed to establish the ratings of the classification systems.

The results of the DEM simulations were compared with elastic solutions. To the authors' knowledge, this is the first verification of DEM calculations for supported openings against available elastic solutions. For the purpose of comparison with elastic solutions, the equivalent shear modulus of the jointed rock mass and rock bolt elastic modulus had to be determined. Estimates for the shear modulus were obtained using standard solutions to make a consistent comparison. No attempt was made to modify the assigned input to improve the comparison. The comparison was encouraging when sufficient support was provided. Although the models employed here are simple, this is believed to be an important milestone, because it suggests that future work using more complex models is feasible.

Finally, we proposed the use of an interaction diagram to evaluate the relative effectiveness of rock bolts and lining thickness in the design of the tunnel support. The engineer can use this interaction diagram to make the optimal design decision given a target maximum allowable convergence. The choice among the possible combinations of input values giving rise to the same amount of convergence, i.e. the amount of rock bolt versus lining thickness, will be done by the engineer accounting for the costs required for rock bolt and lining installation. Also the diagram can help the engineer to gauge the effectiveness of introducing an "increment" of either rock bolt support or lining support on an existing support. So this framework sets out opportunities for investigating important problems in rock tunnelling, in which the composite support system (rock bolts and lining) is considered to be one of the governing variables.

The concepts and approach proposed in this paper have only been illustrated in 2-D plane-strain and for the case of a wished in place support. Therefore, the analyses presented are consistent with the practice of most design standards (Federal Highway Association 2009; British Tunnelling Society 2003), in which well-known solutions proposed by Muir Wood (1975) and Einstein & Schwartz (1979) are still widely used to-date in the preliminary design stage. Therefore, a direct comparison with these analytical solutions can be readily made by practitioners. Like the closed-form solutions of (Muir Wood, 1975; Einstein & Schwartz, 1979), the analyses presented in this article are plane-strain, with 3-D effects being neglected. This implies for instance the neglect of the progressive loss of strength of the rock mass as the excavation proceeds, and rock movements due to the 3D shape of the blocks. However, the approach and concepts discussed in this article could be developed further employing, for the final design stage, 3-D DEM models able to capture the influence of different excavation stages and rock joint orientations relative to the tunnel axis realistically.



## References

- Aksoy, C. O., Kantarci, O., & Ozacar, V. (2010). An example of estimating rock mass deformation around an underground opening using numerical modeling. *International Journal of Rock Mechanics and Mining Sciences*, 47(2), 272-278.
- Bandis, S. C., Lumsden, A. C., & Barton, N. R. (1983). Fundamentals of rock joint deformation. *International Journal of Rock Mechanics and Mining Sciences & Geomechanics Abstracts*, 20(6), 249-268.
- Barla G., Debernardi D. (2009). New viscoplastic model for design analysis of tunnels in squeezing conditions. *Rock Mechanics and Rock Engineering*, 42: 259-288.
- Barla G., Debernardi D., Sterpi D. (2011). Time-dependent modelling of tunnels in squeezing conditions. *International Journal of Geomechanics ASCE*, 12: 697-710.
- Barla G., Einstein H., Kovari K. (2013). Manuscripts using Numerical Discrete Element Methods. *Rock Mechanics and Rock Engineering*, 46(4): 655.
- Barton, N., Lien, R., & Lunde, J. (1974). Engineering classification of rock masses for the design of tunnel support. *Rock Mechanics Felsmechanik Mécanique des Roches*, 6(4), 189-236.
- Barton, N., By, T. L., Chryssanthakis, P., Tunbridge, L., Kristiansen, J., Loset, F., Bhasin, R. K., Westerdahl, H., Vik, G. (1994). Predicted and measured performance of the 62-m span Norwegian-Olympic-Ice-Hockey-Cavern at Gjøvik. *International Journal of Rock Mechanics and Mining Sciences & Geomechanics Abstracts*, 31(6), 617-641.
- Barton, N. (2002). Some new Q-value correlations to assist in site characterisation and tunnel design. *International Journal of Rock Mechanics and Mining Sciences*, 39(2), 185-216.
- Bawden, W. F. (1993). The use of rock mechanics principles in Canadian underground hard rock mine design. *Comprehensive rock engineering*, Vol. 5, 247-290.
- Bhasin, R. K., Barton, N., Grimstad, E., Chryssanthakis, P., Shende, F. P. (1996). Comparison of Predicted and Measured Performance of a Large Cavern in the Himalayas. *International Journal of Rock Mechanics and Mining Sciences*, 33 (6), pp. 607 – 626.
- Bieniawski, Z. T. (1983). Geomechanics classification (RMR system) in design applications to underground excavations. Paper presented at the Proceedings - International Symposium on Engineering Geology and Underground Construction, Lisbon.
- Bobet, A. (2009). Elastic solution for deep tunnels. Application to excavation damage zone and rockbolt support. *Rock Mechanics and Rock Engineering*, 42(2), 147-174.
- Bobet, A., & Einstein, H. H. (2011). Tunnel reinforcement with rockbolts. *Tunnelling and Underground Space Technology*, 26(1), 100-123.
- Boon, C. W. (2013). Distinct Element Modelling of Jointed Rock Masses: Algorithms and Their Verification. D.Phil. Thesis, University of Oxford.
- Boon, C. W., Houlsby, G. T., & Utili, S. (2012). A new algorithm for contact detection between convex polygonal and polyhedral particles in the discrete element method. *Computers and Geotechnics*, Vol. 44: 73-82.

781 Boon, C. W., Houlsby G. T., & Utili S. (2013). A new contact detection algorithm for three  
782 dimensional non-spherical particles. *Powder Technology*, S.I. on DEM, 248: 94-102.

783 Boon, C. W., Houlsby, G. T., & Utili, S. (2014). A novel rock slicing algorithm based on linear  
784 programming. *International Journal of Numerical Methods in Engineering* (under review).

785 British Tunnelling Society (2004). Tunnel Lining Design Guide. Thomas Telford, pp. 179.

786 Brown, E. T. (1981). Putting the NATM into perspective. *Tunnels and Tunnelling International*, 13(10),  
787 13-17.

788 Brown, E. T., Bray, J. W., Ladanyi, B., & Hoek, E. (1983). Ground response curves for rock tunnels.  
789 *Journal of Geotechnical Engineering*, 109(1), 15-39.

790 Cai, M., Kaiser, P.K., Uno, H., Tasaka, Y., Minami, M. (2004). Estimation of rock mass deformation  
791 modulus and strength of jointed hard rock masses using the GSI system. *International Journal of*  
792 *Rock Mechanics and Mining Sciences*, 41(1), 3-19.

793 Carranza-Torres, C., & Fairhurst, C. (1999). The elasto-plastic response of underground excavations  
794 in rock masses that satisfy the hoek-brown failure criterion. *International Journal of Rock Mechanics*  
795 *and Mining Sciences*, 36(6), 777-809.

796 Carranza-Torres, C., & Fairhurst, C. (2000). Application of the convergence-confinement method of  
797 tunnel design to rock-masses that satisfy the Hoek-Brown failure criterion. *Tunnelling and*  
798 *Underground Space Technology*, 15(2), 187-213.

799 Carranza-Torres, C. (2009). Analytical and numerical study of the mechanics of rockbolt  
800 reinforcement around tunnels in rock masses. *Rock Mechanics and Rock Engineering*, 42(2), 175-228.

801 Case, J., & Chilver, A. H. (1971). Strength of Materials and Structures: an Introduction to the  
802 Mechanics of Solids and Structures. Edward Arnold. 2<sup>nd</sup> Edition.

803 Chrysanthakis, P., Barton, N., Lorig, L., & Christianson, M. (1997). Numerical simulation of fiber  
804 reinforced shotcrete in a tunnel using the discrete element method. *International Journal of Rock*  
805 *Mechanics and Mining Sciences & Geomechanics Abstracts*, 34(3-4), 590.

806 Crandall, S. H., Dahl, N. C., & Lardner, T. J. (1978). An introduction to the mechanics of solids (2 ed.).  
807 New York: McGraw Hill.

808 Dahlø, T. S., & Nilsen, B. (1994). Stability and rock cover of hard rock subsea tunnels. *Tunnelling and*  
809 *Underground Space Technology Incorporating Trenchless*, 9(2), 151-158.

810 Delisio, A., Zhao, J., & Einstein, H. H. (2013). Analysis and prediction of TBM performance in blocky  
811 rock conditions at the Lötshberg base tunnel. *Tunnelling and Underground Space Technology*, 33,  
812 131-142.

813 Duncan, J. M., & Goodman, R. E. (1968). Finite element analyses of slopes in jointed rock. Contract  
814 Report S-68-3, U.S. Army Engineers Waterways Experiment Station.

815 Eberhardt, E., Stead, D., & Coggan, J. S. (2004). Numerical analysis of initiation and progressive  
816 failure in natural rock slopes-the 1991 Randa rockslide. *International Journal of Rock Mechanics and*  
817 *Mining Sciences*, 41(1), 69-87.

818 Einstein, H. H., & Schwartz, C. W. (1979). Simplified analysis for tunnel support. *ASCE J Geotech*  
819 *Eng Div*, 105(4), 499-518.

820 Federal Highway Administration (2009). U.S. Department of Transportation - Technical Manual  
821 for Design and Construction of Road Tunnels – Civil Elements. Appendix E – Analytical Closed  
822 Form Solutions. <https://www.fhwa.dot.gov/bridge/tunnel/pubs/nhi09010/appe.cfm>

823 Funatsu, T., Hoshino, T., Sawae, H., & Shimizu, N. (2008). Numerical analysis to better understand  
824 the mechanism of the effects of ground supports and reinforcements on the stability of tunnels  
825 using the distinct element method. *Tunnelling and Underground Space Technology*, 23(5), 561-573.

826 Garga, V. K., & Wang, B. (1993). A numerical method for modelling large displacements of jointed  
827 rocks. II. Modelling of rock bolts and groundwater and applications. *Canadian Geotechnical Journal*,  
828 30(1), 109-123.

829 Goodman, R. E. (1989). *Introduction to Rock Mechanics*, 2<sup>nd</sup> Ed., John Wiley & Sons.

830 Goodman, R. E. (1995). Block theory and its application. *Geotechnique*, 45(3), 383-423.

831 Goodman, R. E., & Shi, G. H. (1985). Block theory and its application to rock engineering. Prentice-  
832 Hall International Series in Civil Engineering and Engineering Mechanics, p. 338.

833 Hammah, R. E., Yacoub, T., Corkum, B., & Curran, J. H. (2008). The practical modelling of  
834 discontinuous rock masses with finite element analysis. American Rock Mechanics Association  
835 (ARMA), 08-180.

836 Hoek, E., & Diederichs, M. (2006). Empirical estimates of rock mass modulus. *International Journal*  
837 *of Rock Mechanics and Mining Sciences*, 42(2), 277-285.

838 Hoek, E., Kaiser, P. K., & Bawden, W. F. (1995). Support of Underground Excavations in Hard Rock:  
839 Taylor & Francis Group, p. 215.

840 Hudson, J. A., & Feng, X. (2010). Technical auditing of rock mechanics modelling and rock  
841 engineering design. *International Journal of Rock Mechanics and Mining Sciences*, 47(6), 877-886.

842 Itasca. (2004). UDEC - Universal distinct element code, ver. 4: Itasca Consulting Group Inc.

843 Ivars, D. M., Pierce, M. E., Darcel, C., Reyes-Montes, J., Potyondy, D. O., Paul Young, R., & Cundall, P.  
844 A. (2011). The synthetic rock mass approach for jointed rock mass modelling. *International Journal of*  
845 *Rock Mechanics and Mining Sciences*, 48(2), 219-244.

846 Jaeger, J. C., Cook, N. G. W., Zimmerman, R. (2007). *Fundamentals of Rock Mechanics*. John Wiley.  
847 4<sup>th</sup> Ed. pp. 488.

848 Jiang, Y., Tanabashi, Y., Li, B., & Xiao, J. (2006). Influence of geometrical distribution of rock joints on  
849 deformational behavior of underground opening. *Tunnelling and Underground Space Technology*,  
850 21(5), 485-491.

851 Jiang, M., & Yin, Z. Y. (2012). Analysis of stress redistribution in soil and earth pressure on tunnel  
852 lining using the discrete element method. *Tunnelling and Underground Space Technology*, 32, 251-  
853 259.

854 Kim, Y. I., Amadei, B., & Pan, E. (1999). Modeling the effect of water, excavation sequence and rock  
855 reinforcement with discontinuous deformation analysis. *International Journal of Rock Mechanics and*  
856 *Mining Sciences*, 36(7), 949-970.

857 Kozicki, J., & Donzé, F. V. (2008). A new open-source software developed for numerical simulations  
858 using discrete modeling methods. *Computer Methods in Applied Mechanics and Engineering*, 197(49-  
859 50), 4429-4443.

860 Kulhawy, F. H. (1978). Geomechanical model for rock foundation settlement. *ASCE J Geotech Eng Div*,  
861 104(2), 211-227.

862 Li, C., & Stillborg, B. (1999). Analytical models for rock bolts. *International Journal of Rock Mechanics*  
863 *and Mining Sciences*, 36(8), 1013-1029.

864 Liu, H. Y., Small, J. C., Carter, J. P., & Williams, D. J. (2009). Effects of tunnelling on existing support  
865 systems of perpendicularly crossing tunnels. *Computers and Geotechnics*, 36(5), 880-894.

866 Londe, P. (1970). Stability of rock slopes – graphical methods. *Journal of the Soil Mechanics and*  
867 *Foundations Divisions*, 96(4), July/August 1970, pp. 1411 – 1434.

868 Lorig, L. J. (1985). A simple numerical representation of fully bonded passive rock reinforcement for  
869 hard rocks. *Computers and Geotechnics*, 1(2), 79-97.

870 Makurat, A. , Barton, N., Vik G., Chryssanthakis, P. and Monsen, K (1990). Jointed rock mass  
871 modelling. *Proc. Int Symp. on Rock Joints*, pp. 657 – 656. Loen, Norway.

872 Malmgren, L., & Nordlund, E. (2008). Interaction of shotcrete with rock and rock bolts-A numerical  
873 study. *International Journal of Rock Mechanics and Mining Sciences*, 45(4), 538-553.

874 Mathews, S.M., Tillman, V.H. and Worotnicki, G. (1983). A modified cablebolt system for support of  
875 underground openings. *Proc. Aust. Inst. Min. Metall. Annual Conf.*, Broken Hill. 243-255.

876 Montgomery, D. C., & Runger, G. C. (2010). *Applied Statistics and Probability for Engineers*: John  
877 Wiley & Sons.

878 Moosavi, M., & Grayeli, R. (2006). A model for cable bolt-rock mass interaction: Integration with  
879 discontinuous deformation analysis (DDA) algorithm. *International Journal of Rock Mechanics and*  
880 *Mining Sciences*, 43(4), 661-670.

881 Metropolitan Transport Authority (2013). *Blasting Concludes Under Grand Central Terminal*. Article  
882 in April 2013. Retrieved from [http://new.mta.info/news/2013/04/12/blasting-concludes-under-](http://new.mta.info/news/2013/04/12/blasting-concludes-under-grand-central-terminal)  
883 [grand-central-terminal](http://new.mta.info/news/2013/04/12/blasting-concludes-under-grand-central-terminal)

884 Nickson, S.D. 1992. Cable support guidelines for underground hard rock mine operations. MASC.  
885 thesis, Dept. Mining and Mineral Processing, University of British Columbia.

886 Oda, M., Yamabe, T., Ishizuka, Y., Kumasaka, H., Tada, H., & Kimura, K. (1993). Elastic stress and  
887 strain in jointed rock masses by means of crack tensor analysis. *Rock Mechanics and Rock*  
888 *Engineering*, 26(2), 89-112.

889 Palmström, A. & Singh, R. (2001). The deformation modulus of rock masses – comparisons between  
890 in situ tests and indirect estimates. *Tunnelling and Underground Space Technology*, 16 (2), 115-131.

891 Pellet, F., & Egger, P. (1996). Analytical model for the mechanical behaviour of bolted rock joints  
892 subjected to shearing. *Rock Mechanics and Rock Engineering*, 29(2), 73-97.

893 Potvin, Y. (1988). Empirical open stope design in Canada. Ph.D., University of British Columbia.

894 Potvin, Y. and Milne, D. (1992). Empirical cable bolt support design. In *Rock Support in mining and*  
895 *underground construction, Proc. Int. Symp. on Rock Support*, Sudbury, (eds P.K. Kaiser and D.R.  
896 McCreath), 269-275. Rotterdam: Balkema.

897 Priest, S. D., & Hudson, J. A. (1976). Discontinuity spacings in rock. *International Journal of Rock*  
898 *Mechanics and Mining Sciences & Geomechanics Abstracts*, 13(5), 135-148.

899 Rabcewicz, L. V. The New Austrian Tunnelling Method, *Water Power*, Vol. 16, No. 11, Nov 1964, pp  
900 453-457.

901 Sjöberg, J., Leander, M., & Saiang, D. (2006). Three-dimensional analysis of tunnel intersections for a  
902 train tunnel under Stockholm. Paper presented at the *Proceedings of the North American Tunneling*  
903 *2006 Conference*, 39-48.

904 Shen, B., & Barton, N. (1997). The disturbed zone around tunnels in jointed rock masses.  
905 *International Journal of Rock Mechanics and Mining Sciences*, 34(1): 117-125.

906 Shi, G. H. (1988). Discontinuous deformation analysis: A new numerical model for the statics and  
907 dynamics of block systems. Ph.D., University of California, Berkeley.

908 Šmilauer, V. (2010). Ph.D. thesis, Cohesive particle model using the discrete element method on the  
909 Yade platform: Czech Technical University, Université Grenoble I.

910 Solak, T. (2009). Ground behavior evaluation for tunnels in blocky rock masses. [doi: DOI:  
911 10.1016/j.tust.2008.10.004]. *Tunnelling and Underground Space Technology*, 24(3), 323-330.

912 Solak, T., & Schubert, W. (2004). Influence of block size and shape on the deformation behavior and  
913 stress development around tunnels. Paper presented at the EUROCK 2004 & 53rd Geomechanics  
914 Colloquium, Salzburg, Austria.

915 Son, M., & Cording, E. J. (2007). Ground–liner interaction in rock tunneling. *Tunnelling and*  
916 *Underground Space Technology*, 22(1), 1-9.

917 Staub, I., Fredriksson, A., & Outters, N. (2002). Strategy for a Rock Mechanics Site Descriptive Model:  
918 Development and testing of the theoretical approach. SKB Report, R02-02. Stockholm, Sweden:  
919 Swedish Nuclear Fuel and Waste Management.

920 Stillborg, B. (1994). Professional users handbook for rock bolting (2 ed.): Trans Tech Publications,  
921 Limited.

922 Steiner, W., & Markus, M. (1996). Design of tunnel liners, how important are bending moments?  
923 Paper presented at the Geotechnical Aspects of Underground Construction in Soft Ground, 15 – 17  
924 April, 1996, London.

925 Utili S., Crosta G.B. (2011). Modelling the evolution of natural slopes subject to weathering: Part I.  
926 Limit analysis approach. *Journal of Geophysical Research – Earth Surface*, 116, F01016.

927 Utili S., Crosta G.B. (2011) Modelling the evolution of natural slopes subject to weathering: Part II.  
 928 Discrete element approach. *Journal of Geophysical Research – Earth Surface*, 116, F01017.

929 Vardakos, S. S., Gutierrez, M. S., & Barton, N. R. (2007). Back-analysis of Shimizu Tunnel No. 3 by  
 930 distinct element modeling. *Tunnelling and Underground Space Technology*, **22**(4), 401-413.

931 Wang, H. N., Li, Y., Ni, Q., Utili, S., Jiang, M. J., & Liu F. (2013). Analytical solutions for the  
 932 construction of deeply buried circular tunnels with two liners in rheological rock. *Rock mechanics  
 933 and rock engineering*, **46**(6): 1481-1498.

934 Wang, H. N., Utili, S., Jiang, M. J. (2014). An analytical approach for the sequential excavation of  
 935 circular tunnels in rheological rock. *International Journal of Rock Mechanics and mining Science*, in  
 936 press, DOI: RMMS2910.

937 Yeung, M. R., & Leong, L. L. (1997). Effects of joint attributes on tunnel stability. [doi: DOI:  
 938 10.1016/S1365-1609(97)00286-4]. *International Journal of Rock Mechanics and Mining Sciences*,  
 939 34(3-4), 348.e341-348.e318.

940 Zangerl, C., Eberhardt, E., Evans, K. F., & Loew, S. (2008). Consolidation settlements above deep  
 941 tunnels in fractured crystalline rock: Part 2-numerical analysis of the gotthard highway tunnel case  
 942 study. *International Journal of Rock Mechanics and Mining Sciences*, 45(8), 1211-1225.

943 Zhang, L. (2010). Method for estimating the deformability of heavily jointed rock masses. *Journal of  
 944 Geotechnical and Geoenvironmental Engineering ASCE*, 136(9), 1242-1250.

945

## TABLES

Table 1: Failure mechanisms for different joint orientations and friction angles.

No.	Joint orientations			Friction angle	Failure Mechanism 1	Failure Mechanism 2
	A	B	C			
1	60°E	40°E	80°W	35°	Roof fall – wedge subtended by joint sets with largest acute relative angle	N/A
2	10°E	30°W	50°W	35°	Roof fall – wedge subtended by joint sets with largest acute relative angle	Toppling at opposite side wall – along most shallow joint set
3	80°E	5°E	65°W	35°	Roof fall – wedge subtended by joint sets with largest acute relative angle	Sliding at opposite sidewall – wedge subtended by other joint sets
4	20°W	60°W	80°W	35°	Roof fall – wedge subtended by joint sets with largest acute relative angle	Roof fall – random blocks sliding along the steepest joint set
5	40°E	20°E	50°W	35°	Roof fall – blocks sliding along steepest joint set	Sliding at sidewall – blocks sliding along most shallow joint set
6	55°E	25°E	45°W	35°	Roof fall – blocks sliding along second steepest joint set	N/A
7	60°E	80°E	40°W	35°	Roof fall – minor block falling without distinct pattern	Sliding at sidewall – blocks sliding along most shallow joint set
8	75°E	55°E	65°W	35°	Roof fall – wedge subtended by joint sets with largest acute relative angle	Sliding propagates along two opposite directions after wedge falls
9	60°E	85°E	80°W	25°	Roof fall – minor block fall without distinct pattern	N/A
10	5°E	55°E	15°W	30°	Roof fall – blocks sliding along steepest joint set	Toppling at sidewall along second steepest joint set
11	85°E	75°E	65°W	25°	Roof fall – wedge subtended by joint sets with largest acute relative angle	N/A
12	85°E	75°E	65°W	35°	Roof fall – minor block fall without distinct pattern	N/A
13	85°E	75°E	55°W	30°	Roof fall – wedge subtended by joint sets with largest acute relative angle	Sliding propagates along two opposite directions after wedge falls
14	85°E	75°E	55°W	35°	Roof fall – minor block fall without distinct pattern	Sliding at sidewall – blocks sliding along most shallow joint set
15	85°E	75°E	45°W	30°	Roof fall – minor block fall without distinct pattern	Sliding at sidewall – blocks sliding along most shallow joint set
16	85°E	75°E	45°W	35°	Roof fall – minor block fall without distinct pattern	Sliding at sidewall – blocks sliding along most shallow joint set
17	85°E	75°E	35°W	35°	Roof fall – minor block fall without distinct pattern	Sliding at sidewall – blocks sliding along most shallow joint set
18	75°E	25°W	75°W	35°	Roof fall – block fall without distinct pattern	Sliding at sidewall – minor block fall along most shallow joint set
19	75°E	25°W	55°W	35°	Roof fall – wedge subtended by joint sets with largest acute relative angle	Sliding propagates along two opposite directions after wedge falls
20	75°E	25°W	45°W	35°	Roof fall – blocks sliding along steepest joint set	Sliding at sidewall – minor block fall along most shallow joint set
21	75°E	25°E	25°W	35°	Roof fall – blocks sliding along steepest joint set	Sliding at sidewall – minor block fall along most shallow joint set
22	75°E	45°E	25°W	35°	Roof fall – blocks sliding along steepest joint set	Sliding at sidewall – blocks sliding along second steepest joint set
23	75°E	85°E	25°W	35°	Roof fall – minor block fall without distinct pattern	Sliding at sidewall – blocks sliding along most shallow joint set
24	85°E	70°E	45°E	25°	Roof fall – wedge subtended by joint sets with largest acute relative angle	N/A

952 Table 2: Parameters used in the numerical model.

Parameters	Values
Cover depth	20 m
Diameter of opening/tunnel, D	10 m
Density of rock	2700 kg/m <sup>3</sup>
Rock joint normal stiffness, $k_n$	5 GPa/m
Rock joint shear stiffness, $k_s$	0.5 GPa/m
Bolt axial stiffness, $K_a$	0.2 GN/m
Ultimate tensile strength of rock bolts	500 kN
Joint friction angle, $\phi$	35°
Joint dilation angle, $\psi$	0°
Friction angle at the rock – lining interface, $\phi_L$	30 °
Normal and tangential contact stiffness between lining and rock, $K_L$	1 GPa/m
Lining elastic modulus, $E_L$	25 GPa
Joint orientations:	
Joint set 1	dip direction = East, dip angle = 75°
Joint set 2	dip direction = East, dip angle = 25°
Joint set 2	dip direction = West, dip angle = 25°
Standard deviation of the dip angle for each joint set	1°
Joint centre intensity (number of joint centres per unit area in 2-D) for each joint set	1 joint/m <sup>2</sup>
Minimum block size (minimum radius of the largest inscribed circle)	0.5 m

953

954 Table 3: Estimated shear moduli using different approaches.

Ref. No.	Method of estimation	Poisson's ratio, $\nu$	Shear modulus, $G$ (GPa)
G1	$G = k_s s_{\text{mean}}$	0.2 (assumed)	0.385
G2	$G = k_n s_{\text{mean}} / (2(1+\nu))$	0.2 (assumed)	1.604
G3	1D compression test on the full domain (fig. 1), $\phi=35$ $G = (\sigma_1 - \sigma_3) / 2\varepsilon_1$	0.37 (obtained)	0.527
G4	1D compression test on the full domain (fig. 1), $\phi=89$ $G = (\sigma_1 - \sigma_3) / 2\varepsilon_1$	0.37 (obtained)	0.529
G5	1D compression test on reduced sample size of 20m x 20m, $\phi=35$ $G = (\sigma_1 - \sigma_3) / 2\varepsilon_1$	0.36 (obtained)	0.542
G6	1D compression test on reduced sample size of 10m x 10m, $\phi=35$ $G = (\sigma_1 - \sigma_3) / 2\varepsilon_1$	0.36 (obtained)	0.536
G7	1D compression test on the full domain, horizontal direction, $\phi=35$ $G = (\sigma_1 - \sigma_3) / 2\varepsilon_1$	0.35 (obtained)	0.649
G8	1D compression test along horizontal direction on reduced sample size of 10m x 10m, $\phi=35$ , $G = (\sigma_1 - \sigma_3) / 2\varepsilon_1$	0.35 (obtained)	0.648

955  
956



## FIGURES

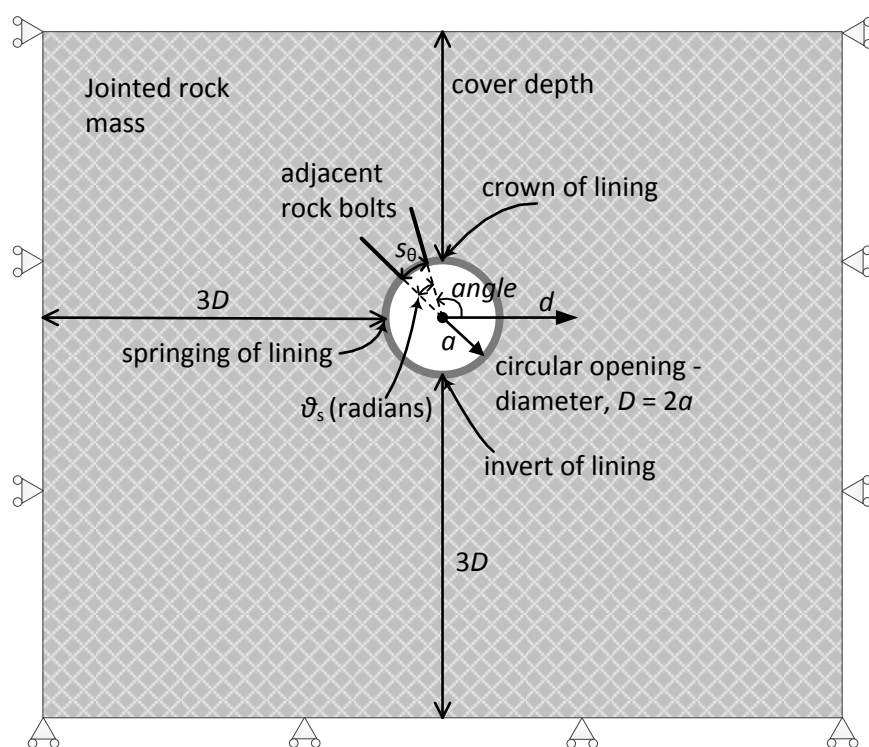
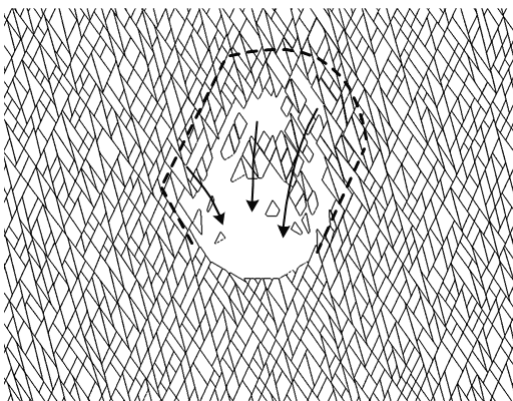


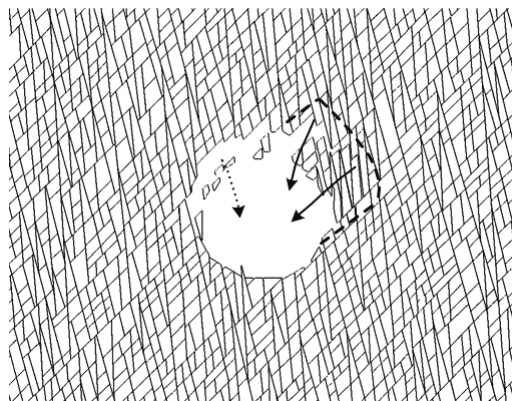
Fig. 1. Schematic of the supported tunnel.

963

(a)

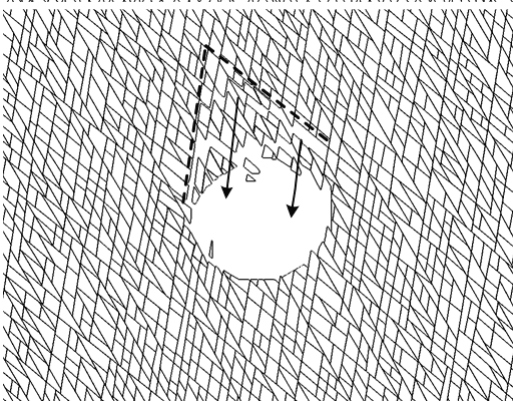


(b)

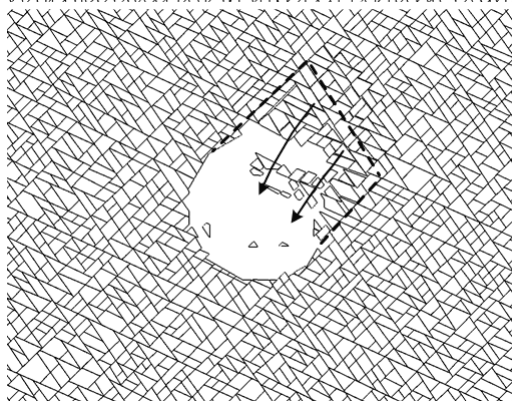


964

(c)

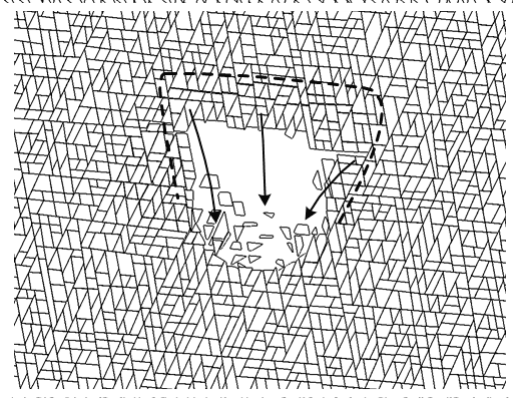


(d)



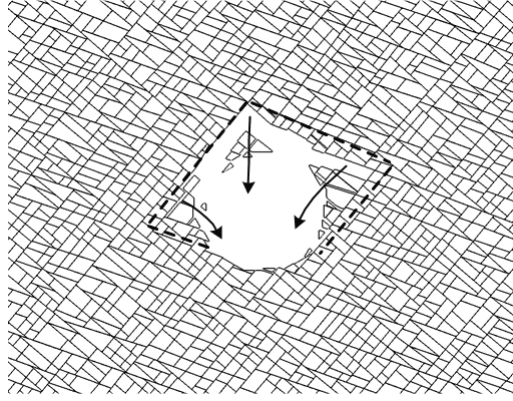
965

(e)

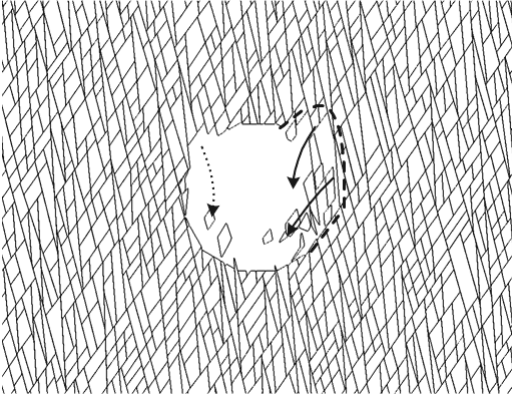


966

(f)



(g)



967

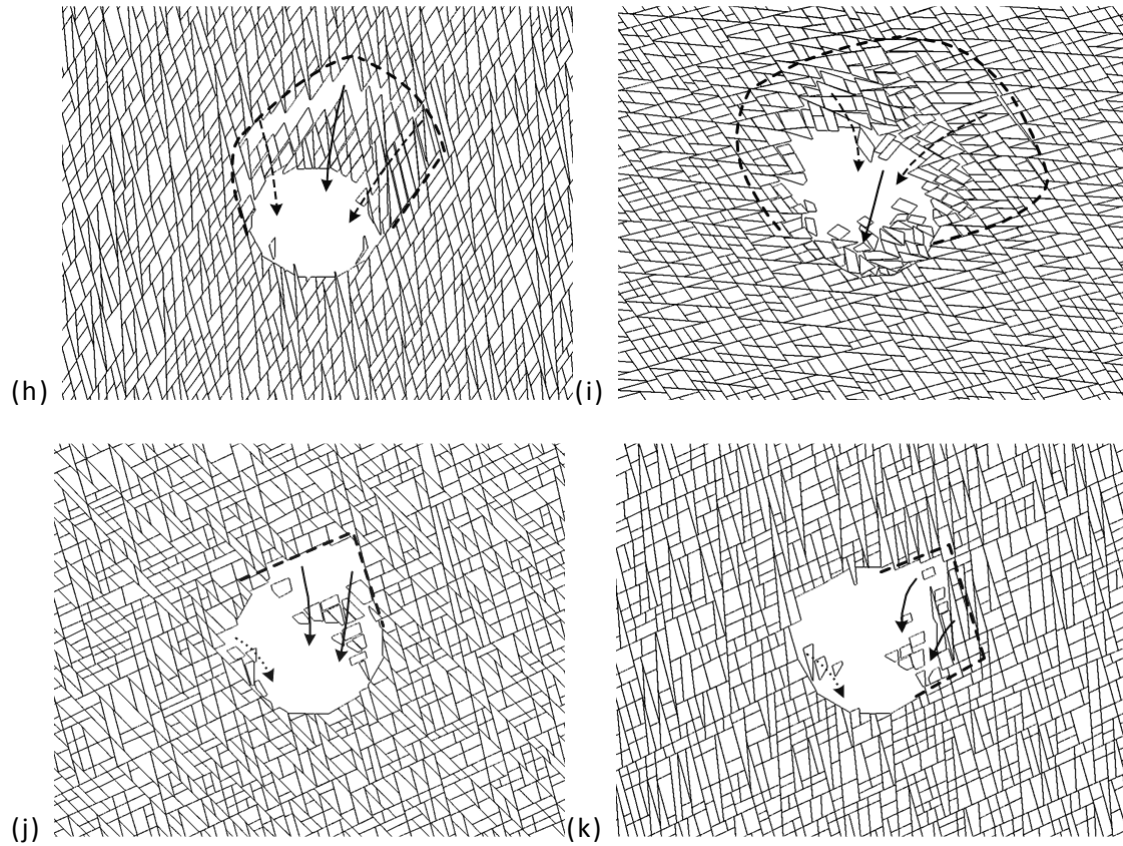


Fig. 2. Failure patterns for different joint patterns. (a) Roof failure (No. 8 in Table 1), joint pattern:  $75^{\circ}\text{E}, 55^{\circ}\text{E}, 65^{\circ}\text{W}$ ,  $\phi_{\text{joint}} = 35^{\circ}$ , (b) side wall failure (No. 16 in Table 1), joint pattern:  $75^{\circ}\text{E}, 85^{\circ}\text{E}, 45^{\circ}\text{W}$ ,  $\phi_{\text{joint}} = 35^{\circ}$ , (c) sliding along the steepest joint set (No. 1 in Table 1), joint pattern:  $60^{\circ}\text{E}, 40^{\circ}\text{E}, 80^{\circ}\text{W}$ ,  $\phi_{\text{joint}} = 35^{\circ}$ , (d) sliding along the second steepest joint set (No. 6 in Table 1), joint pattern:  $55^{\circ}\text{E}, 25^{\circ}\text{E}, 45^{\circ}\text{W}$ ,  $\phi_{\text{joint}} = 35^{\circ}$ , (e) failure involving all joint sets (No. 3 in Table 1), joint pattern:  $80^{\circ}\text{E}, 5^{\circ}\text{E}, 65^{\circ}\text{W}$ ,  $\phi_{\text{joint}} = 35^{\circ}$ , (f) sliding along the steepest joint set led to failure at the roof and eastern side wall, and sliding along the shallowest joint set led to failure at the western sidewall (No. 5 in Table 1), joint pattern:  $40^{\circ}\text{E}, 20^{\circ}\text{E}, 50^{\circ}\text{W}$ ,  $\phi_{\text{joint}} = 35^{\circ}$ , (g) sliding along the most shallow joint set led to sidewall failure (No. 14 in Table 1), and there are minor rock falls from the roof, joint pattern:  $75^{\circ}\text{E}, 85^{\circ}\text{E}, 55^{\circ}\text{W}$ ,  $\phi_{\text{joint}} = 35^{\circ}$ , (h) evolution of failure pattern for joint pattern (the first failure mode is denoted by the solid arrow, which in-turn evolved or propagated into more complex failure modes denoted by the dashed arrows.) (No. 13 in Table 1) :  $75^{\circ}\text{E}, 85^{\circ}\text{E}, 55^{\circ}\text{W}$ ,  $\phi_{\text{joint}} = 30^{\circ}$ , (i) evolution of failure pattern for joint pattern (No. 10 in Table 1):  $5^{\circ}\text{E}, 55^{\circ}\text{E}, 15^{\circ}\text{W}$ ,  $\phi_{\text{joint}} = 30^{\circ}$ , (j) roof failure for joint pattern (No. 22 in Table 1):  $75^{\circ}\text{E}, 45^{\circ}\text{E}, 25^{\circ}\text{W}$ ,  $\phi_{\text{joint}} = 35^{\circ}$ , (k) side wall failure for joint pattern (No. 23 in Table 1):  $75^{\circ}\text{E}, 85^{\circ}\text{E}, 25^{\circ}\text{W}$ ,  $\phi_{\text{joint}} = 35^{\circ}$

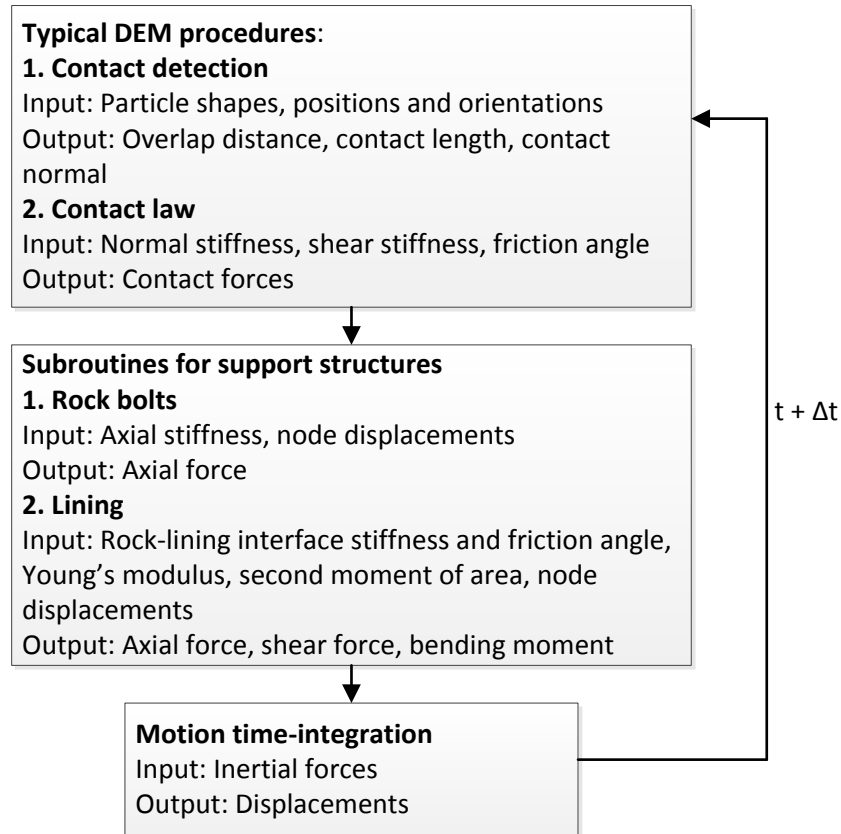
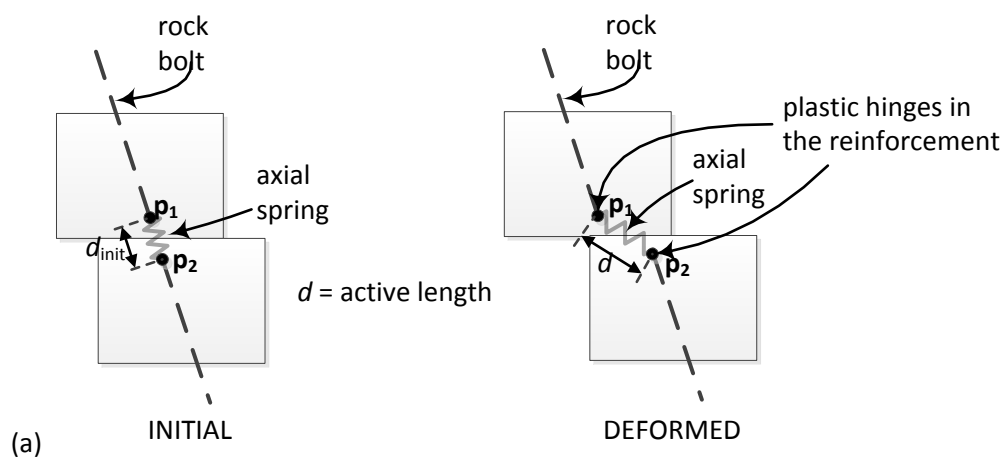


Fig.3. The location of support subroutines in a DEM code



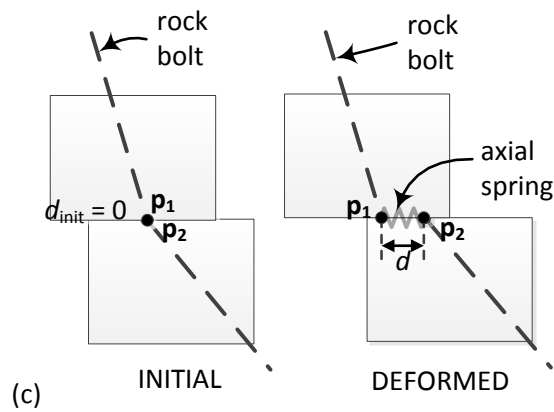
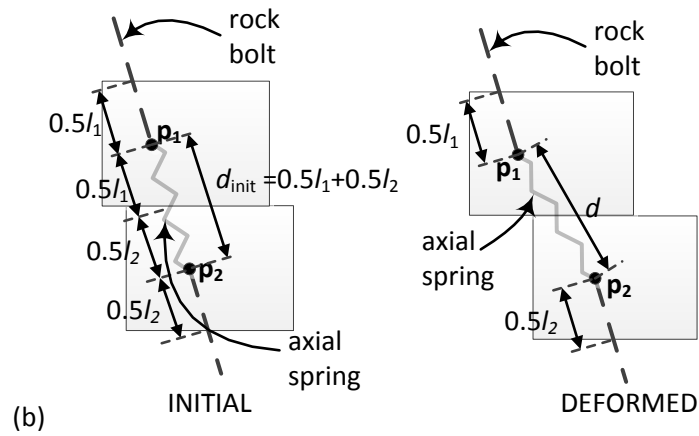
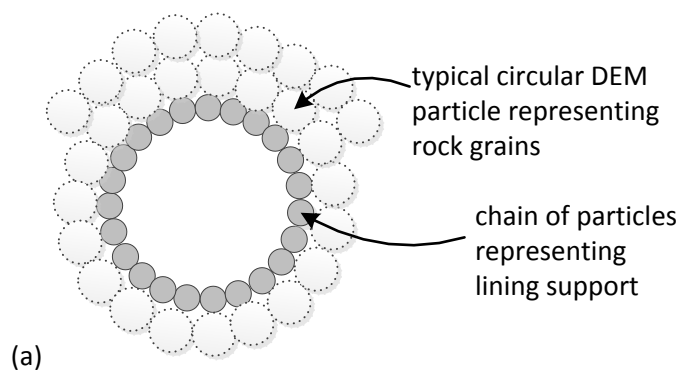
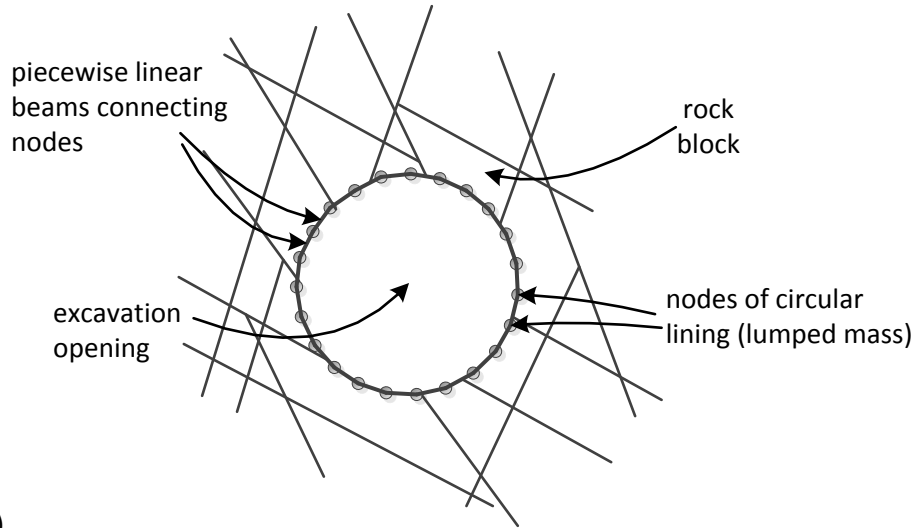


Fig. 4. Rock bolts algorithms. Choices of anchor point located (a) at a prescribed distance from the block face, (b) midway inside the rock block, (c) at the rock joint interface. The initial and deformed configurations of a rock bolt intersecting a pair mating rock blocks are shown.





(b)

Fig. 5. Different approaches to model a tunnel lining using (a) a chain of geometrical entities or (b) nodes connected using piecewise linear beams

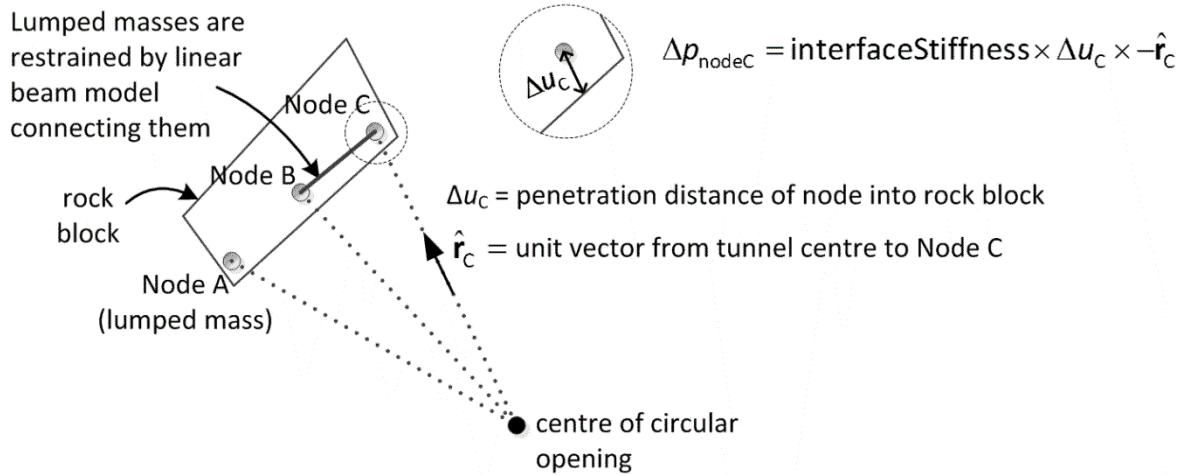
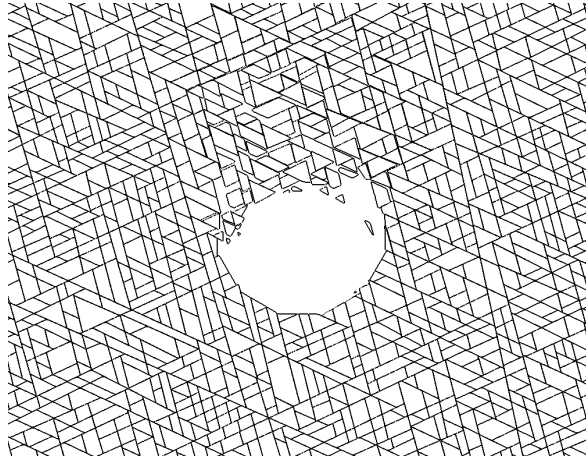
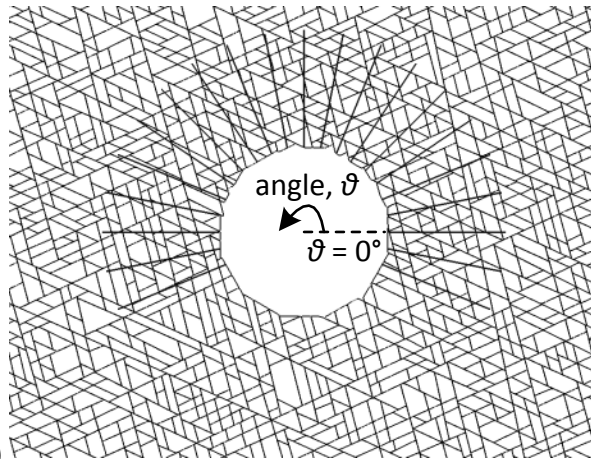


Fig. 6. Nodes forming a segment of lining. External contact forces on the nodes are calculated from the overlaps with the rock block. Forces in the beam between nodes are calculated as in Case & Chilver (1971)

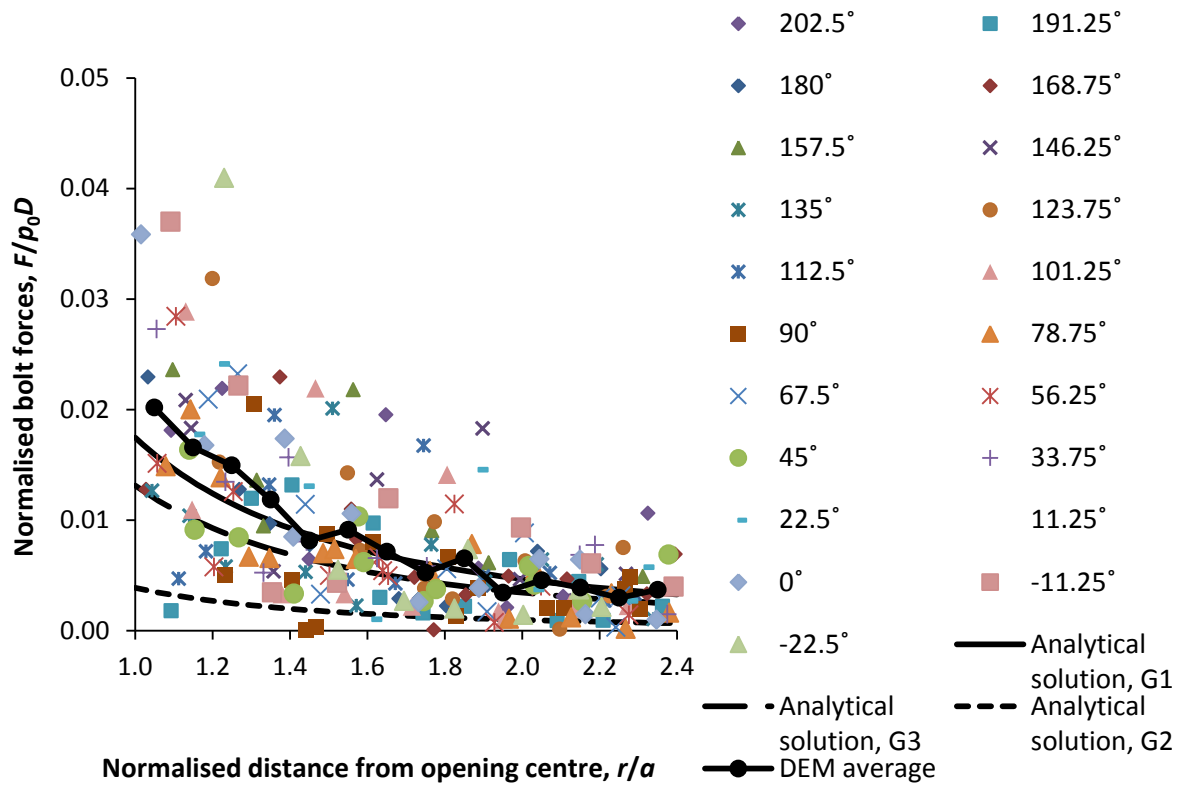


(a)

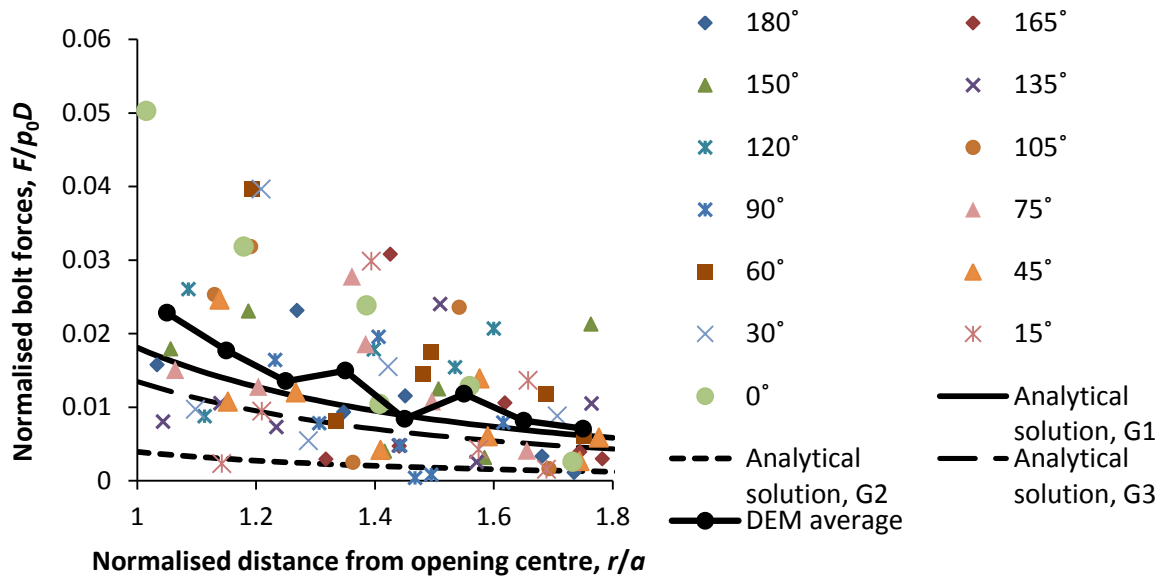


(b)

Fig. 7. Example case, joint pattern 75°E, 25°E, 25°W: (a) without support showing unsupported collapse mechanism, (b) supported dense bolt pattern (bolt length is  $0.7 \cdot D = 7$  m, spacing is 11.25°).

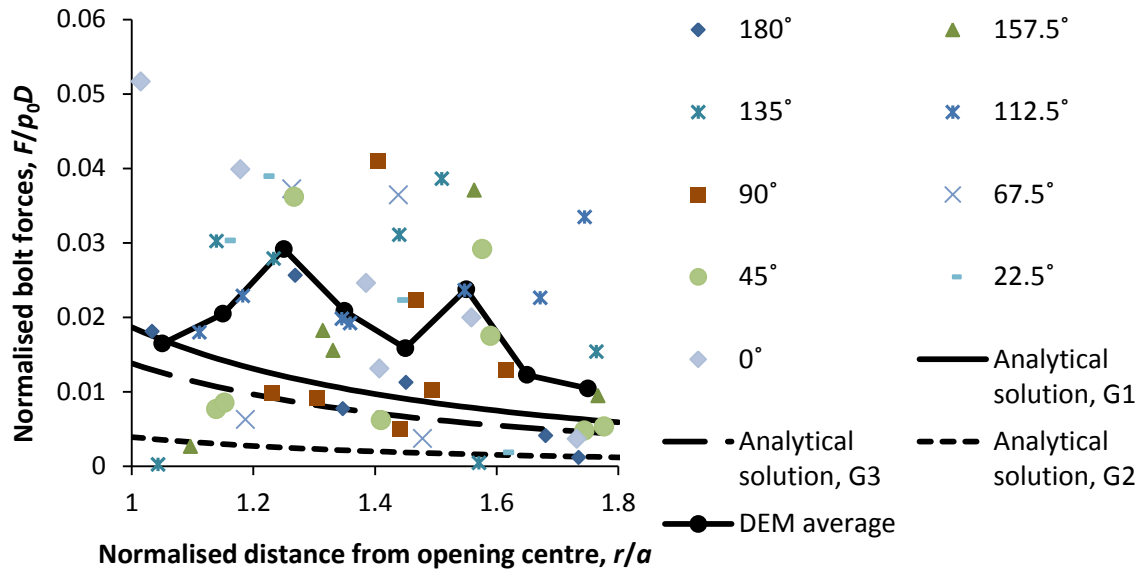


(a)



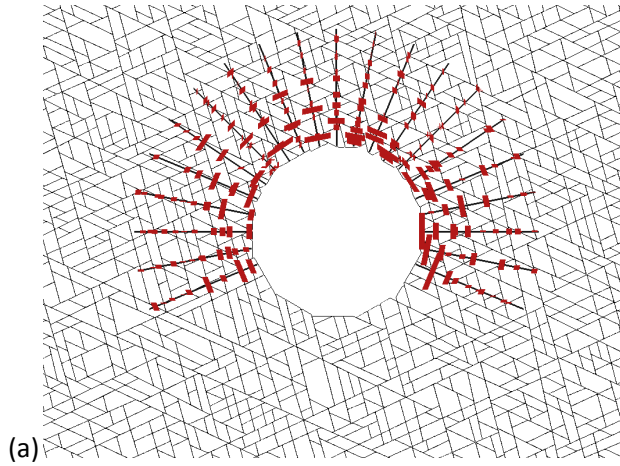
(b)

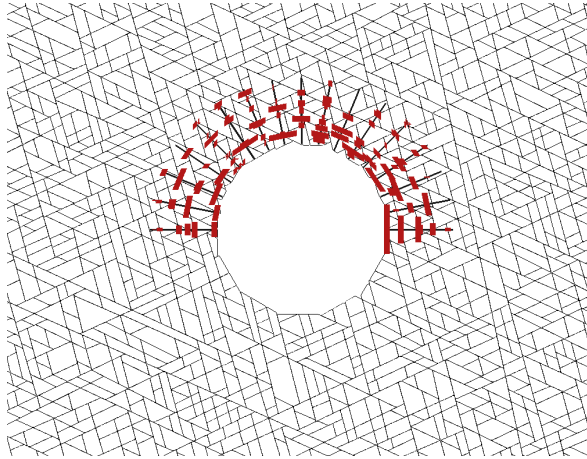




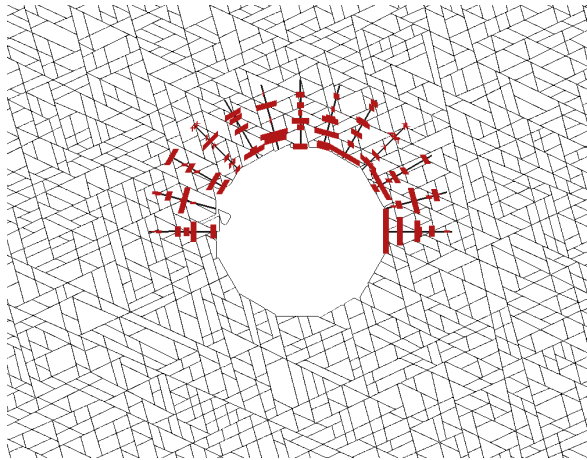
(c)

Fig. 8. Comparison of DEM calculations against analytical solutions proposed by Carranza-Torres (2009) for bolt configuration: (a) 7 m length 11.25° spacing (Fig. 9 a), (b) 4 m length 15° spacing (Fig. 9 c), and (c) 4 m length 22.5° spacing (Fig. 9 c). The averages were taken between  $r/a$  intervals of 0.1. Shear moduli were estimated using approaches summarised in Table 3.

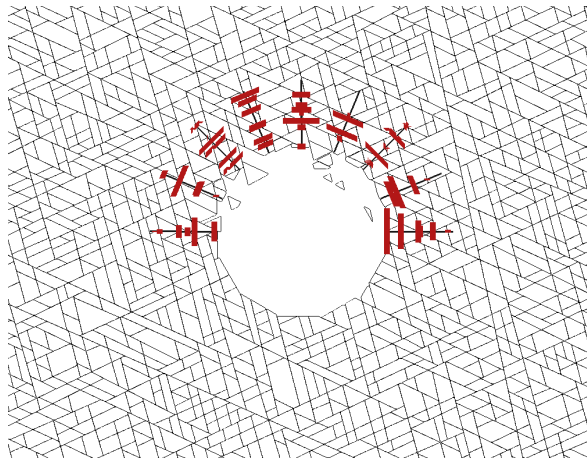




(b)

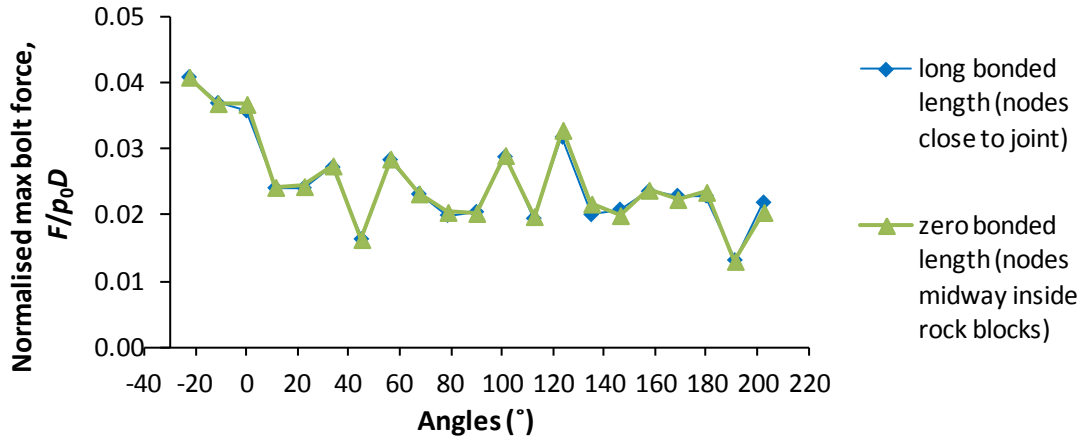


(c)

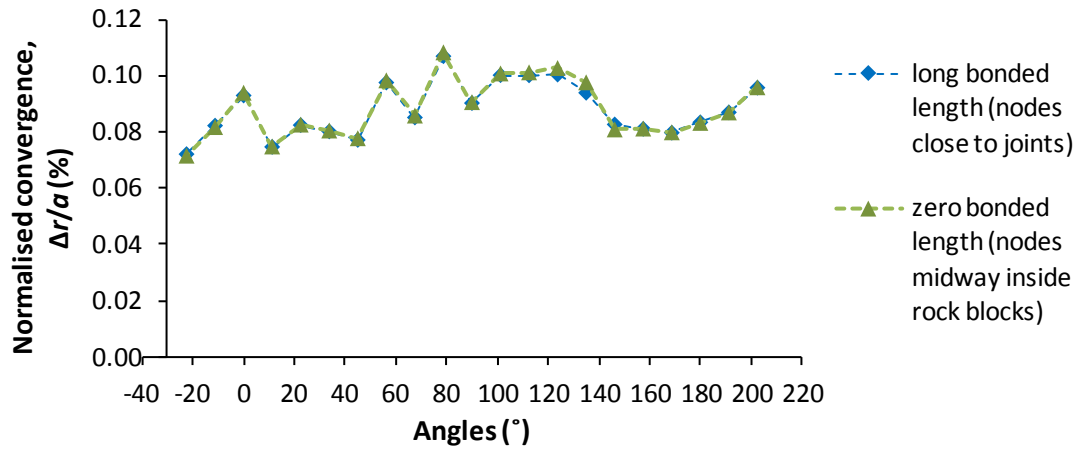


(d)

Fig. 9. Several trials of rock bolt configurations. (a) first trial: long and dense bolt pattern (length 7 m, spacing  $11.25^\circ$ ), (b) second trial: length 4m, spacing  $11.25^\circ$ , (c) third trial: length 4m, spacing  $15^\circ$  spacing, (d) fourth trial: length 4m, spacing  $22.5^\circ$ . The magnitudes of bolt axial forces (red bars perpendicular to the bolts) are all drawn using the same scale.



(a)



(b)

Fig. 10. Comparison of between two rock bolt two rock bolt node choices in terms of (a) maximum bolt forces, and (b) normalised displacements

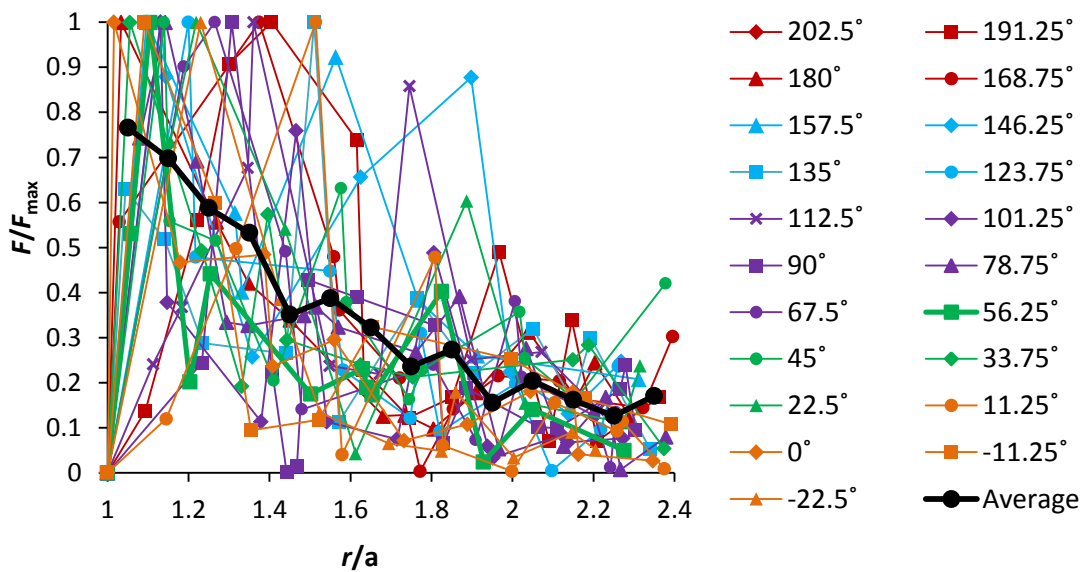
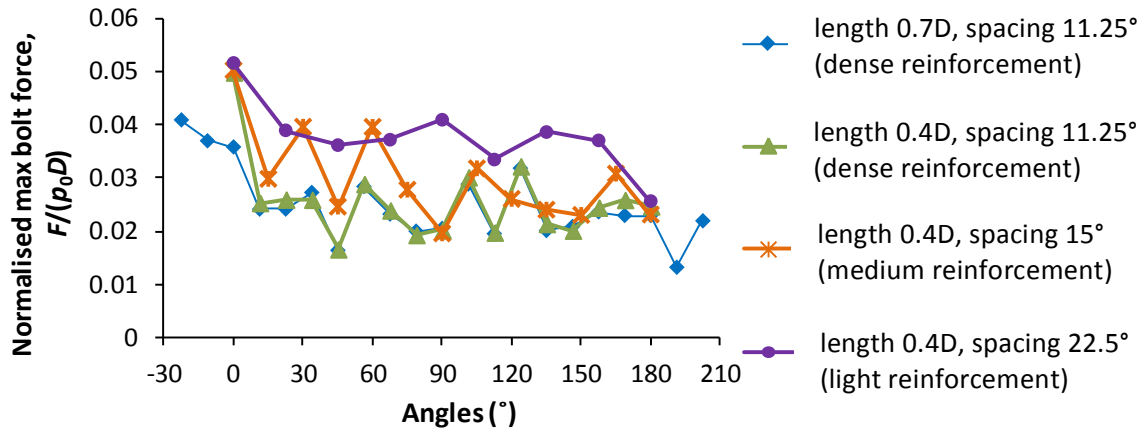
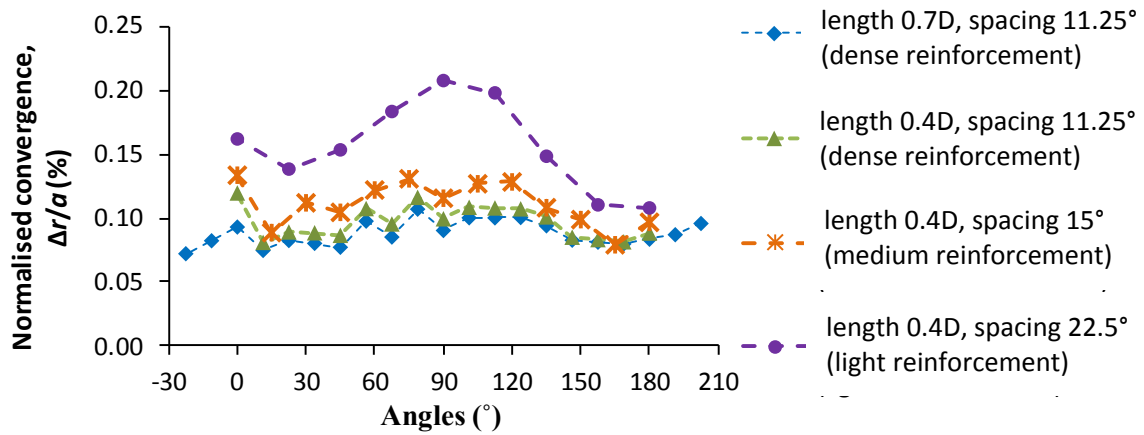


Fig. 11.  $F/F_{\max}$  versus ratio of radial distance from tunnel centre over tunnel radius for each bolt employed. The average was taken between  $r/a$  intervals of 0.1.



(a)



(b)

Fig. 12. Influence of bolt length (7m and 4m) and spacing (11.25°; 15°; 22.5°) on (a) maximum bolt forces and (b) displacements.

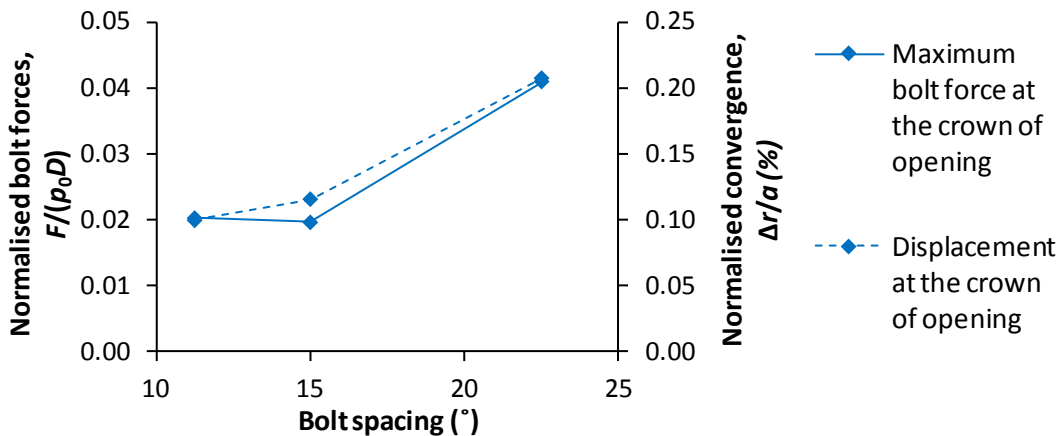
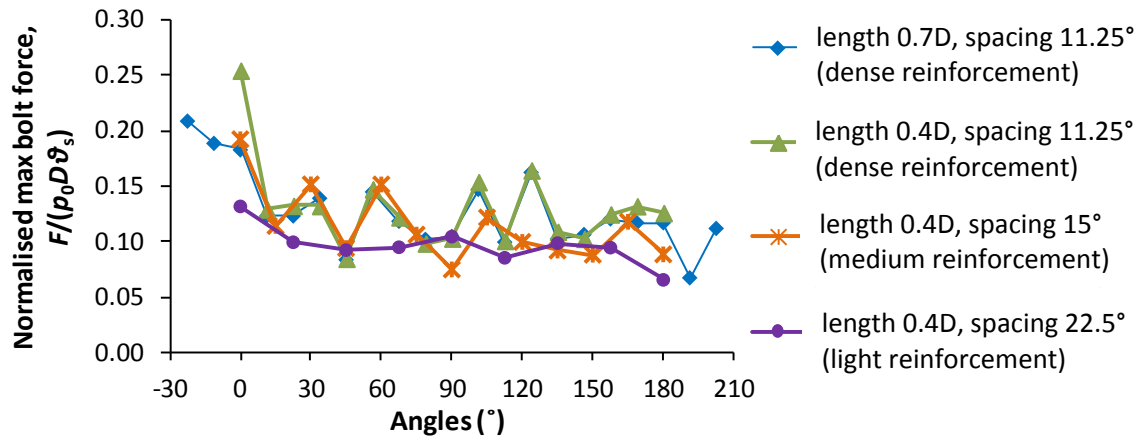
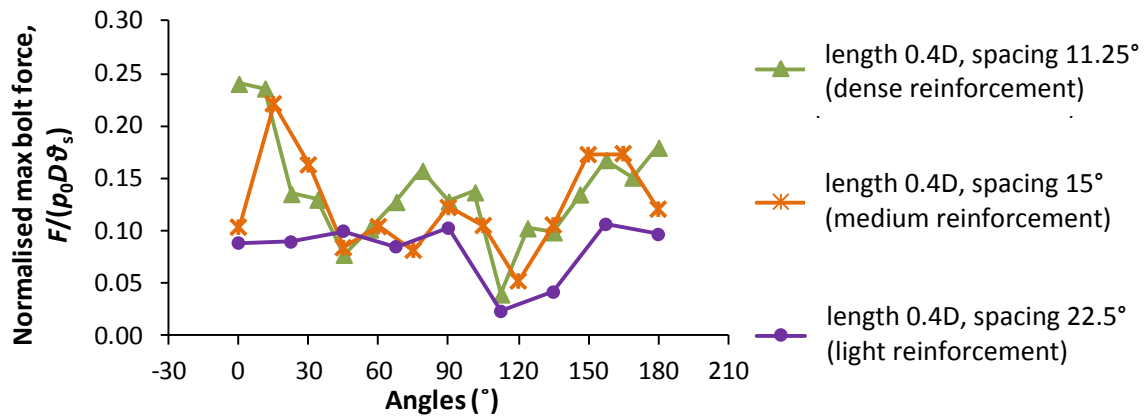


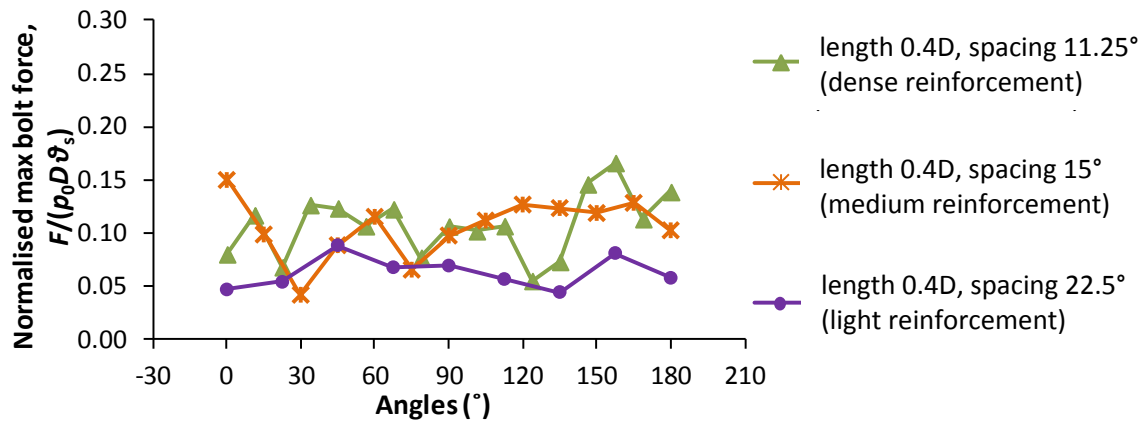
Fig. 13. Bolt forces and displacements at the crown with bolt spacing (bolt length = 4m)



(a)

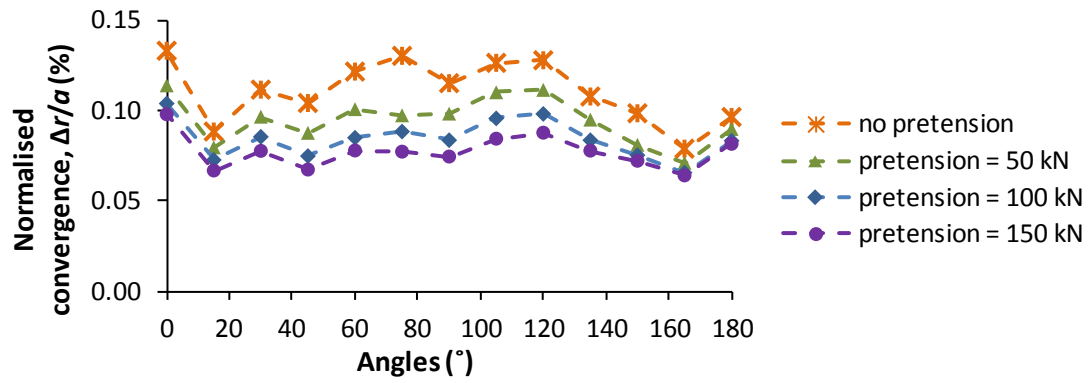


(b)

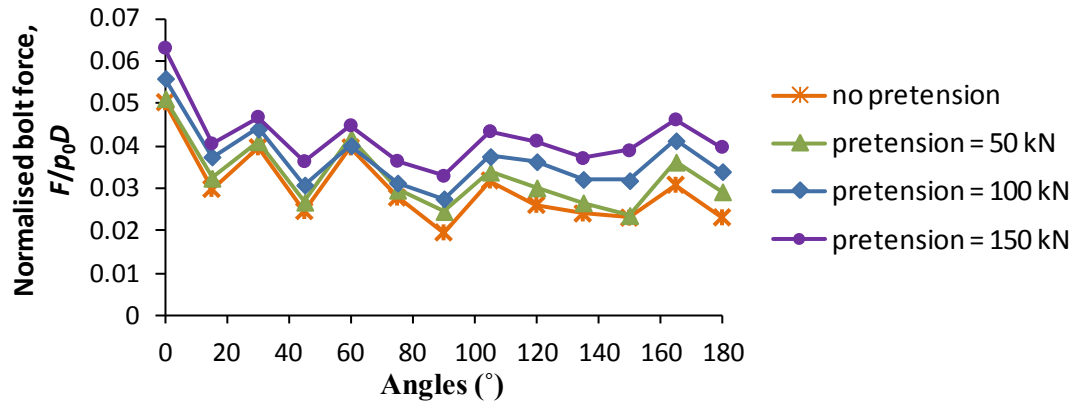


(c)

Fig. 14. Maximum bolt forces normalised against tangential spacing for different bolt length (7m and 4m) and spacing (11.25°; 15°; 22.5°): (a) joint pattern from central analysis, while (b) and (c) are derived from joint patterns generated from the same statistical properties

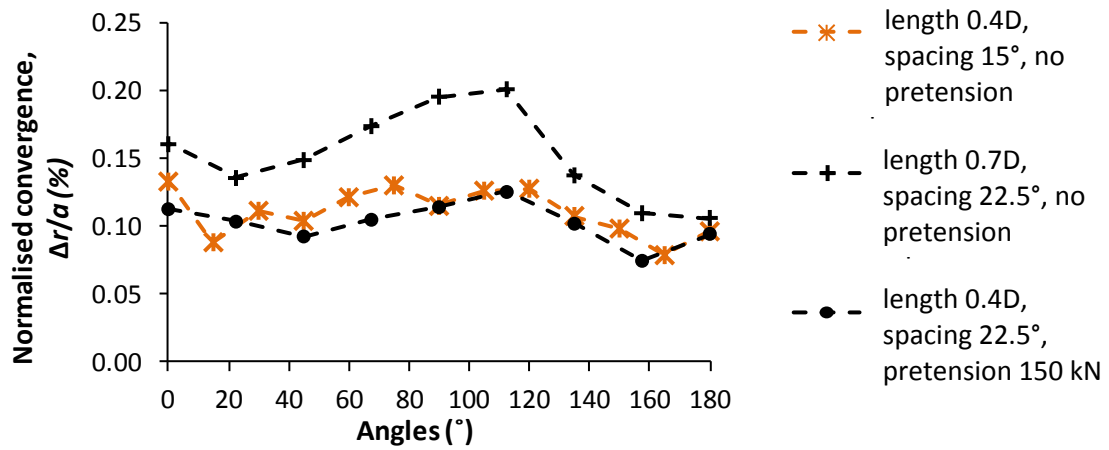


(a)



(b)

Fig. 15. Influence of pretension in terms of (a) tunnel convergence and (b) bolt forces



(a)

(b)

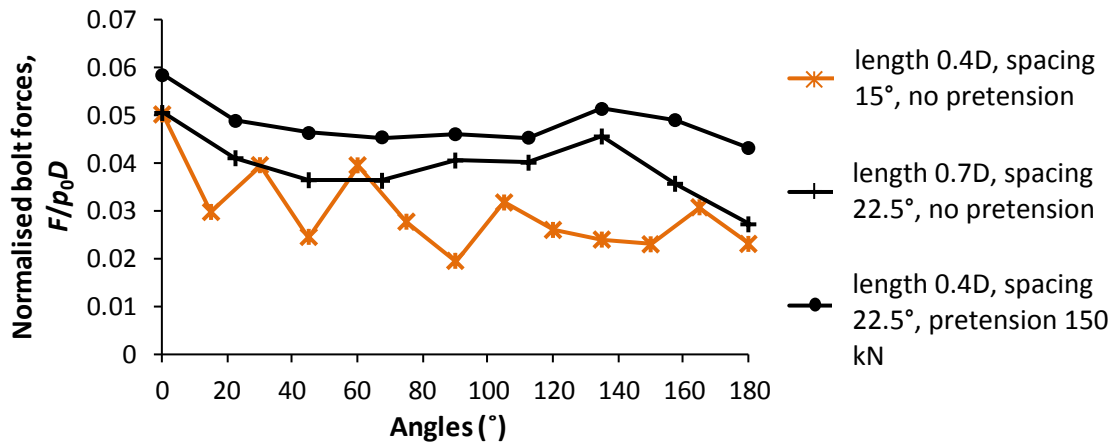


Fig. 16. Comparison of (a) displacements and (b) forces for non-optimal spacing with longer bolts (7m) and with pre-tension.

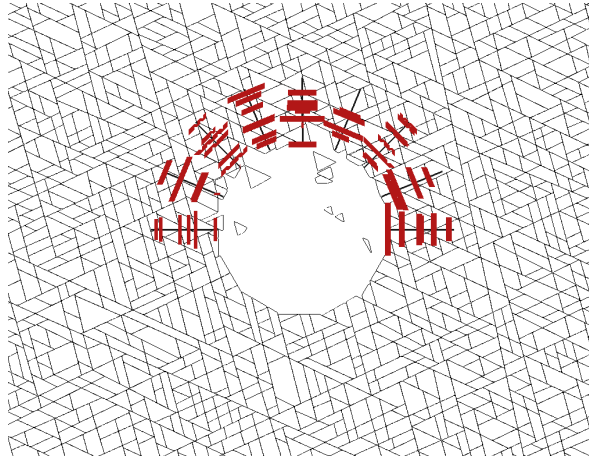
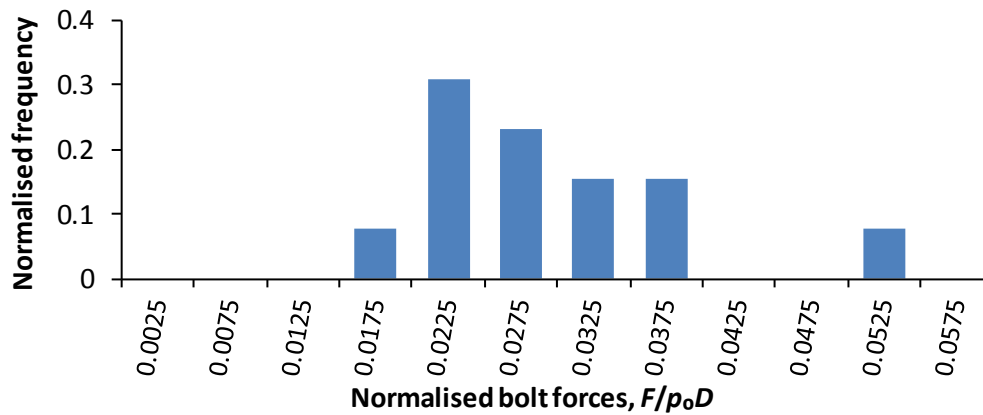
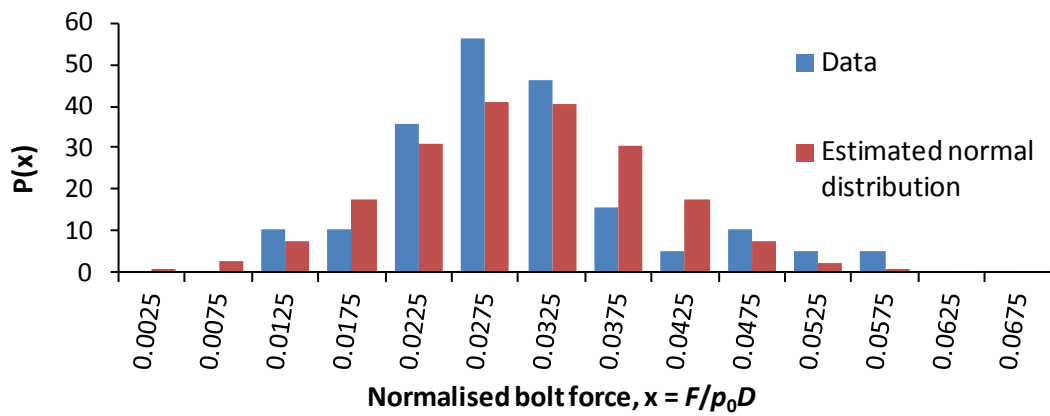
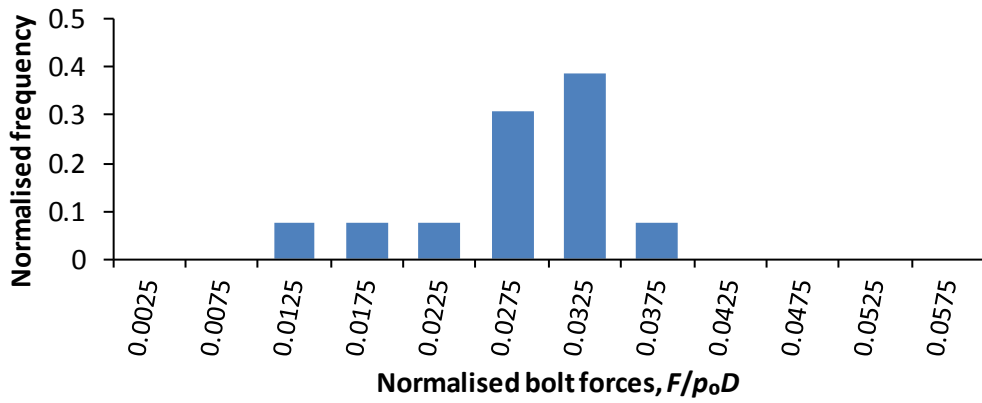
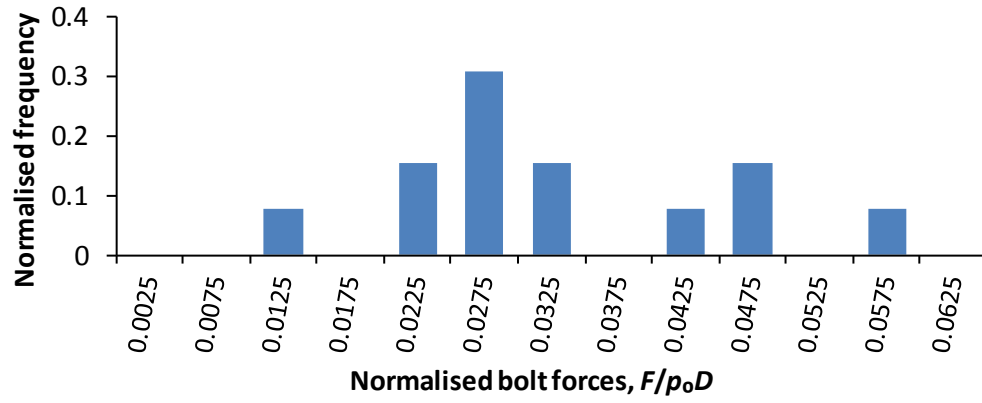


Fig. 17. Use of 150 kN pretension for rock bolts with 22.5° spacing

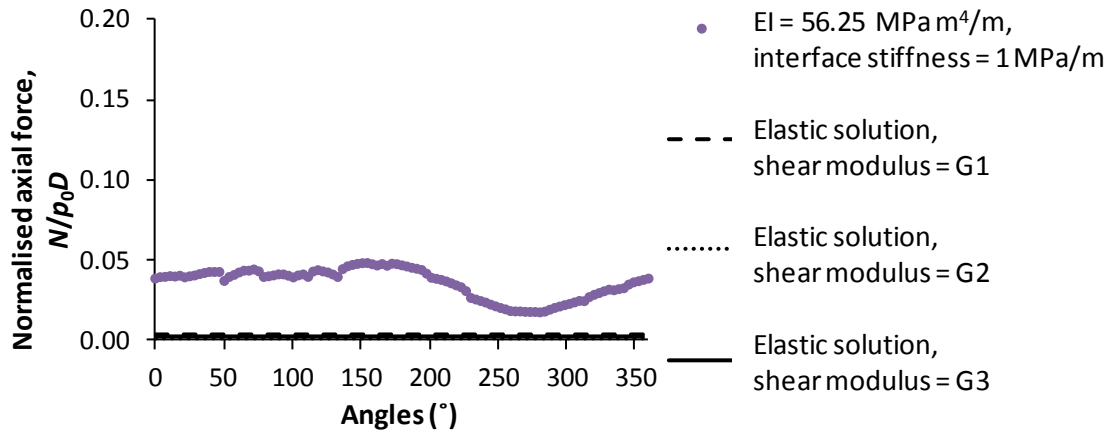


(a)

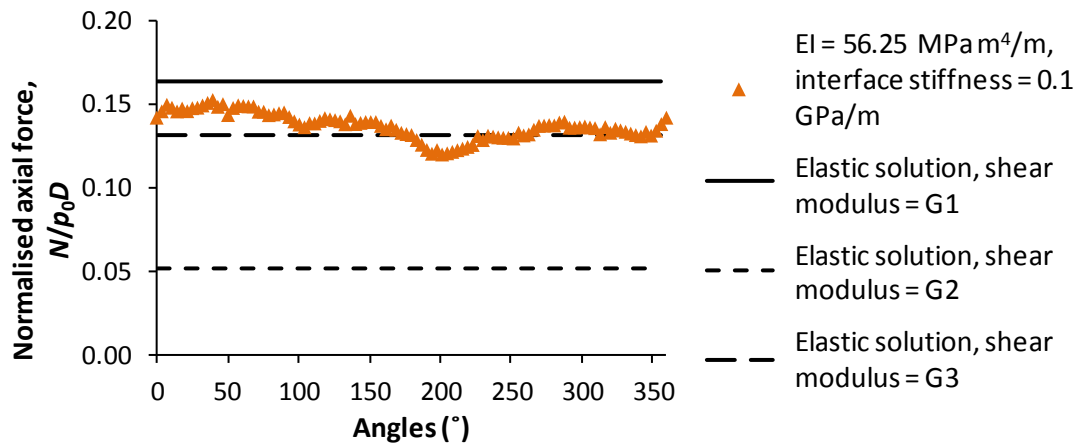


(d) Fig. 18. Histogram of frequency distribution for bolt forces (a) reference sample (mean = 0.030, standard deviation = 0.008), (b) sample B (mean = 0.032, standard deviation = 0.012), (c) sample C (mean = 0.028, standard deviation = 0.007), (d) merged sample, and estimated normal distribution with mean = 0.03 and standard deviation = 0.009.



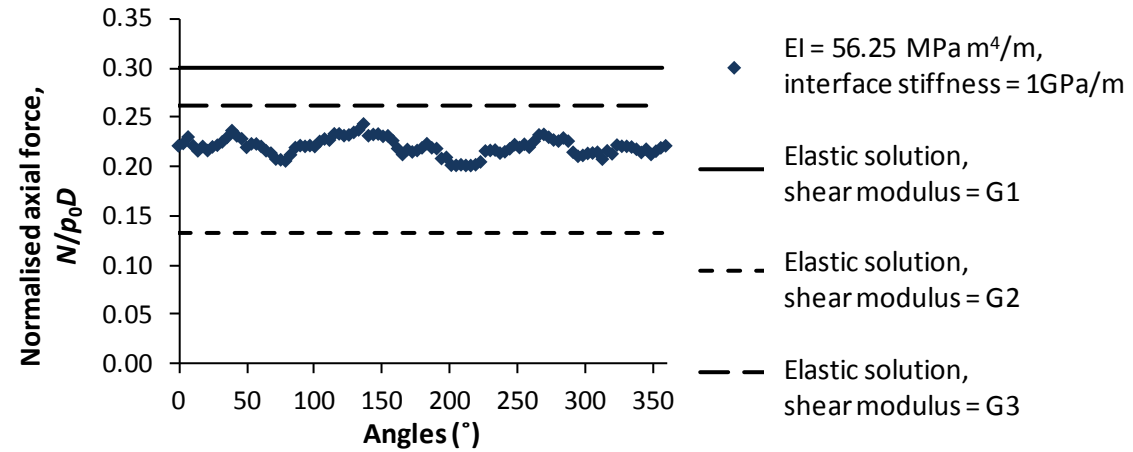


1127 (a)



1128 (b)

1129



1130 (c)

1131 Fig. 19. Comparison between elastic solution for lining axial force and beam forces recorded  
 1132 between lining nodes in DEM calculations for different lining-rock interface stiffness (a) 1 MPa/m, (b)  
 1133 0.1 GPa/m, (c) 1 GPa/m. Shear moduli were estimated using the approaches summarised in Table 3

1134

1135

1136

1137

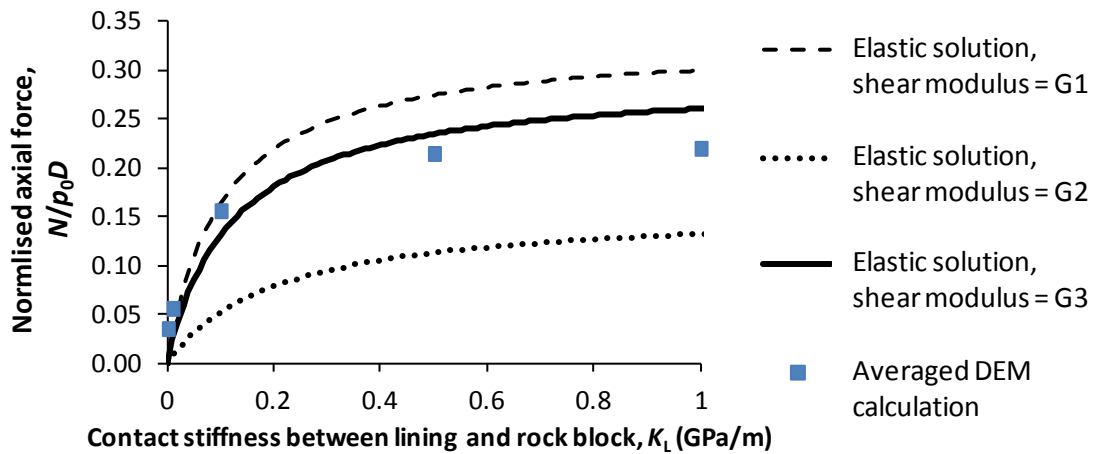
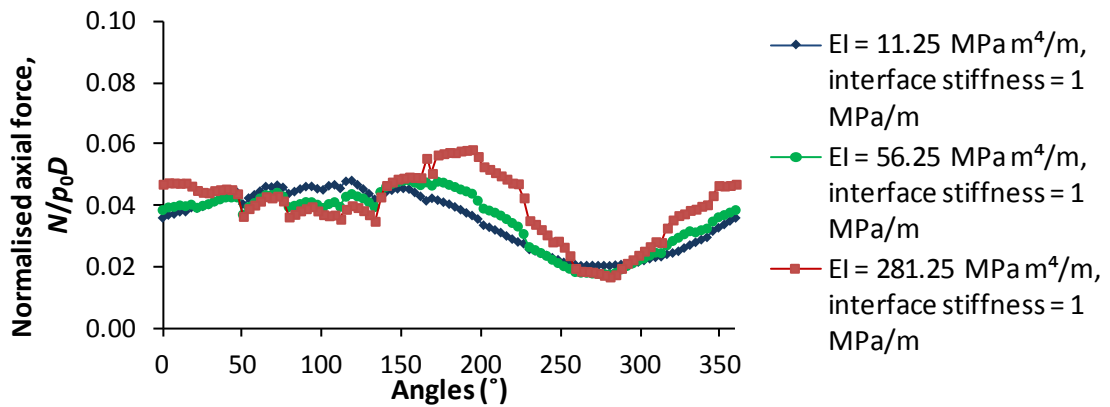
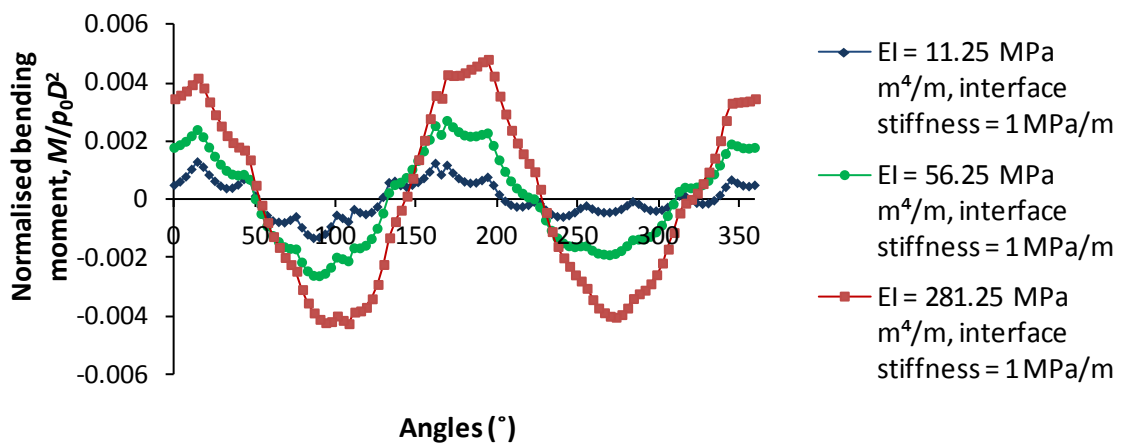


Fig. 20. Comparison between DEM calculations and elastic solutions on lining axial force for different lining-rock interface stiffnesses.



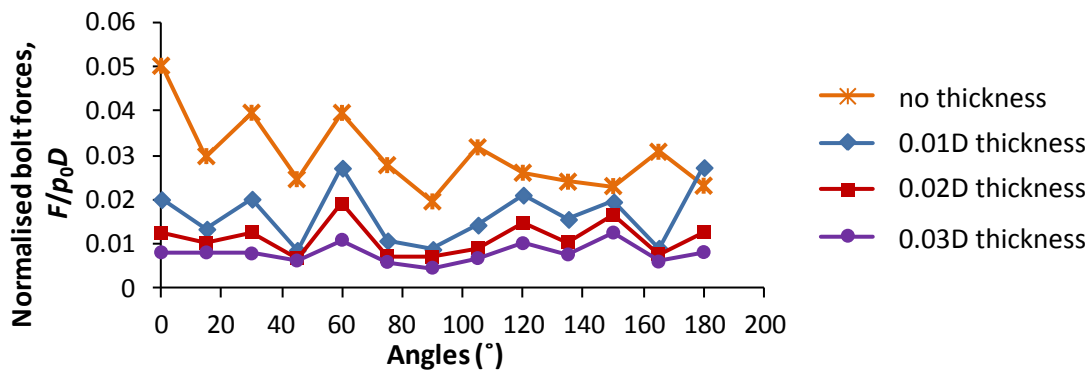
(a)



(b)

Fig. 21. Influence of bending stiffness on lining (a) axial force and (b) bending moment

(a)



(b)

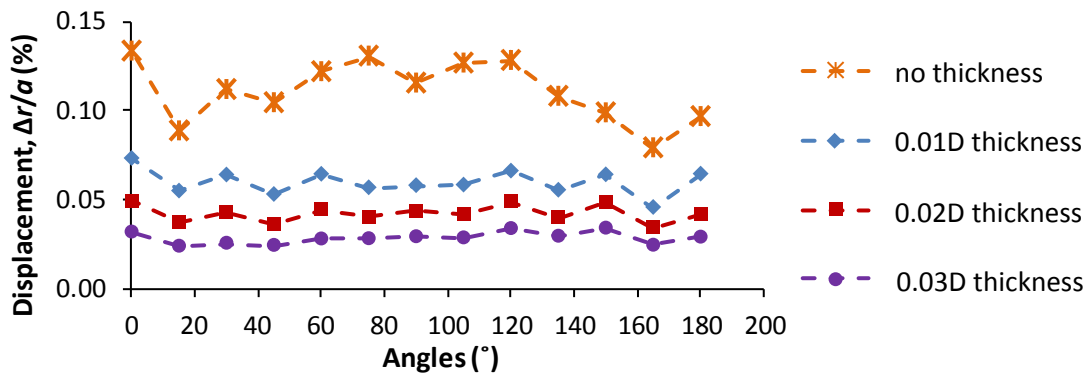
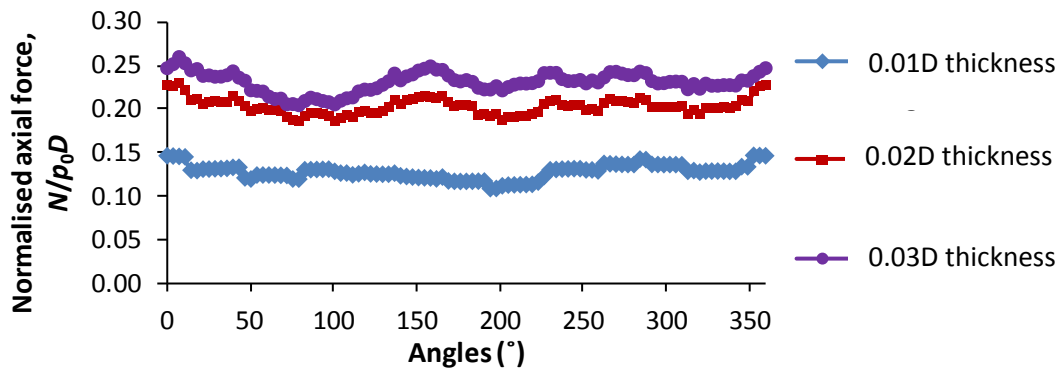
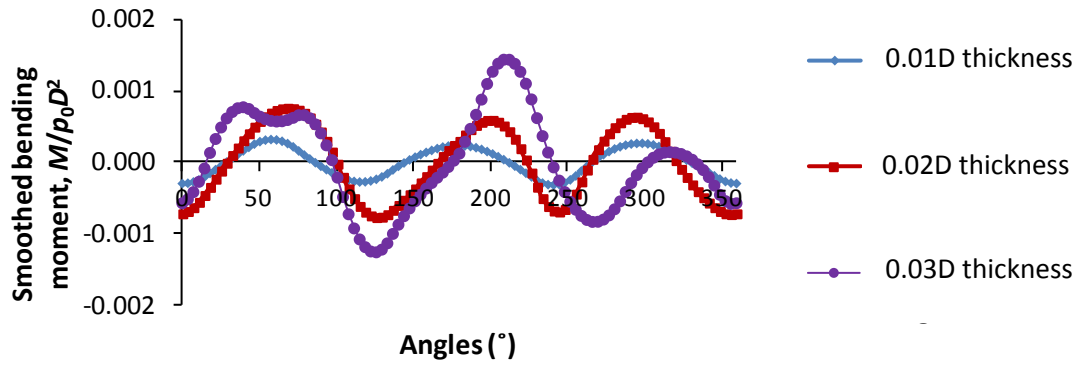


Fig. 22. Influence of lining thickness on (a) bolt forces and (b) tunnel convergence

(a)





(b)  
Fig. 23. (a) Axial forces and (b) bending moments of lining for different thickness of lining (4 m bolt length, 15° spacing) (correction procedures of bending moment for polygonal approximation of circular opening are referred to Boon (2013))

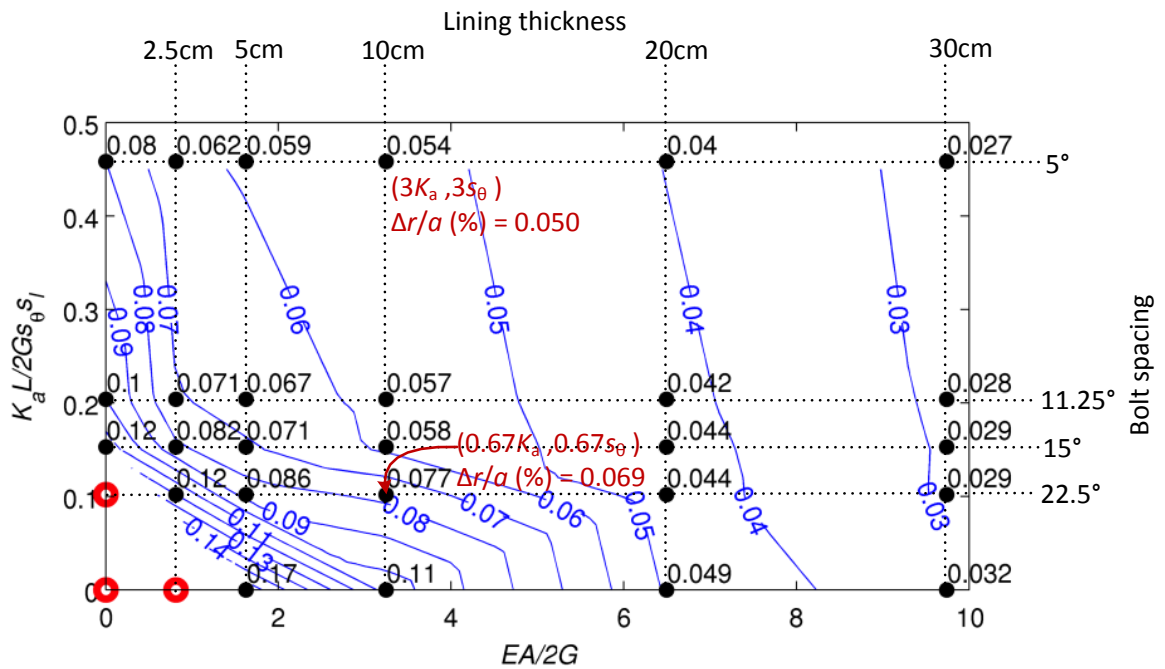


Fig. 24. Interaction diagram showing contours of convergence  $\Delta r/a$  (%) at the crown for different combinations of lining thickness (horizontal axis) and bolt spacing (vertical axis). Red circles denote failure.

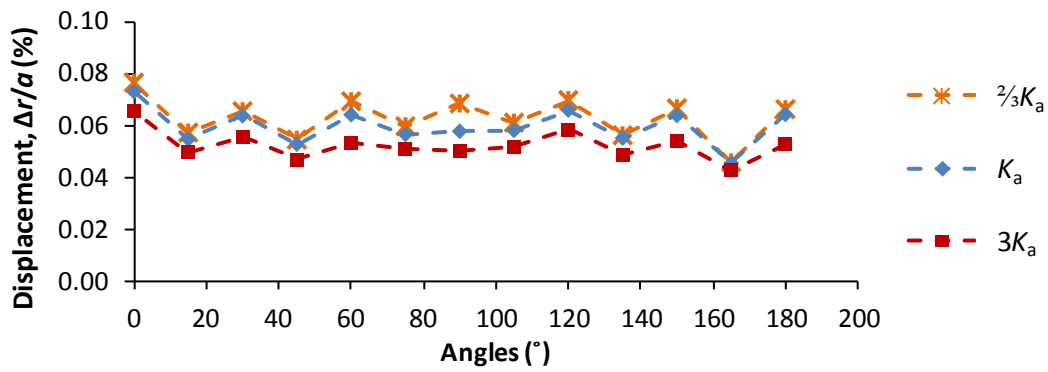
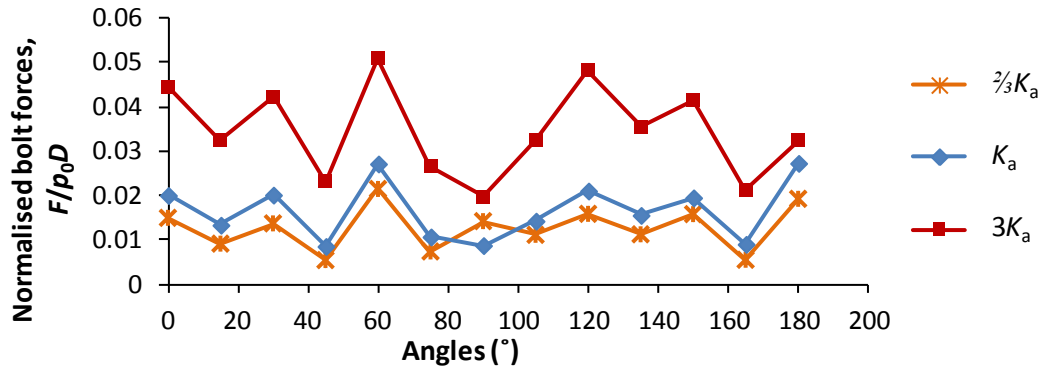


Fig. 25. (a) Bolt forces (b) displacements for different bolt axial stiffness

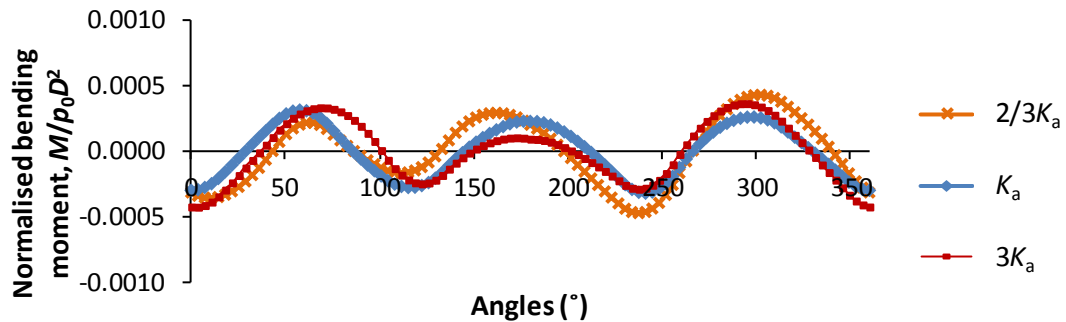
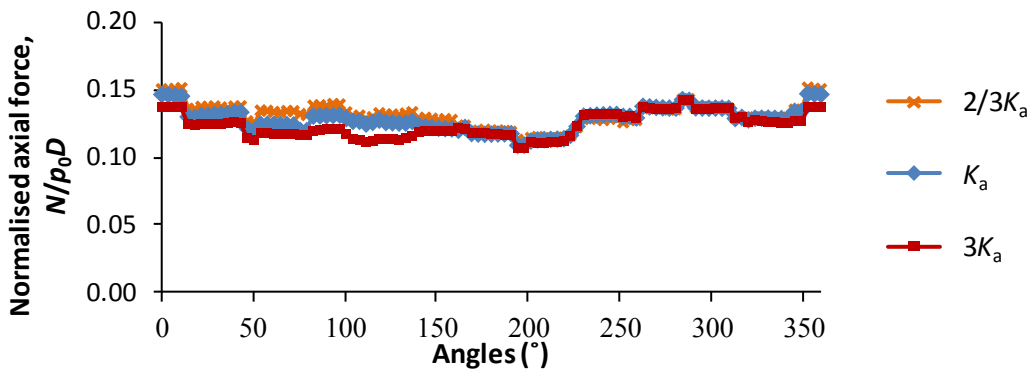


Fig. 26. Influence of bolt axial stiffness on lining (a) axial forces and (b) bending moments for different bolt axial stiffness (4m bolt length, 15° bolt spacing, 10 cm lining) (correction procedures of bending moment for polygonal approximation of circular opening are referred to Boon (2013))

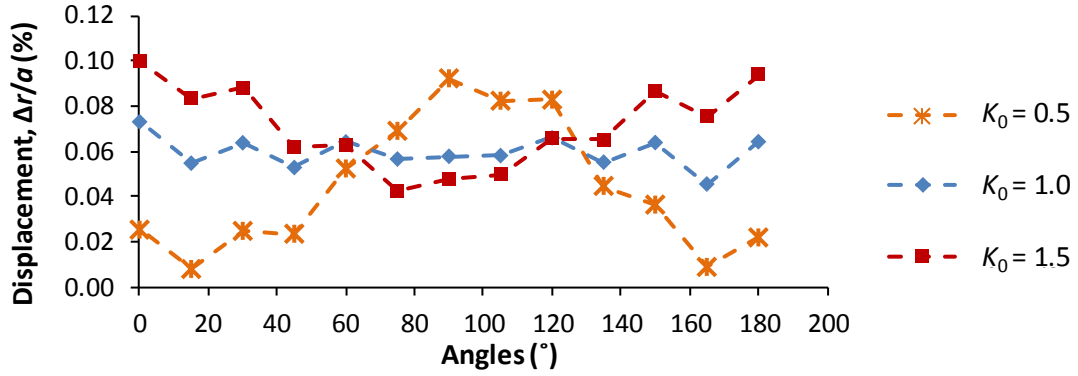
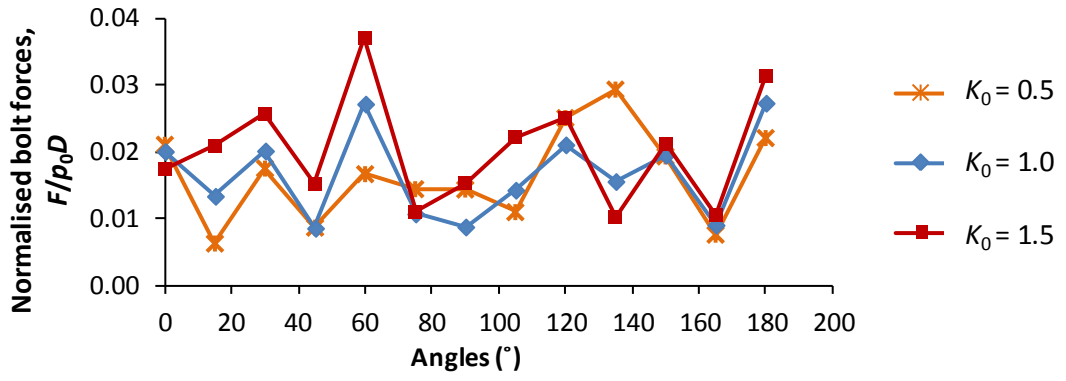


Fig. 27. Bolt (a) stresses and (b) displacements for different in-situ stresses  $K_0$

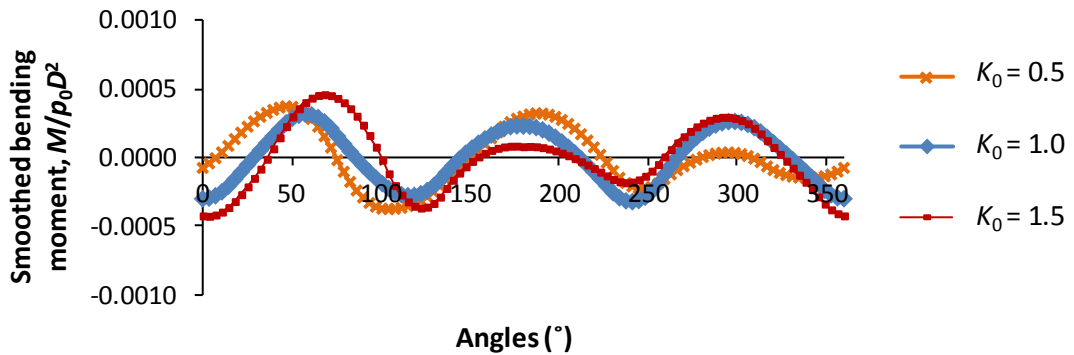
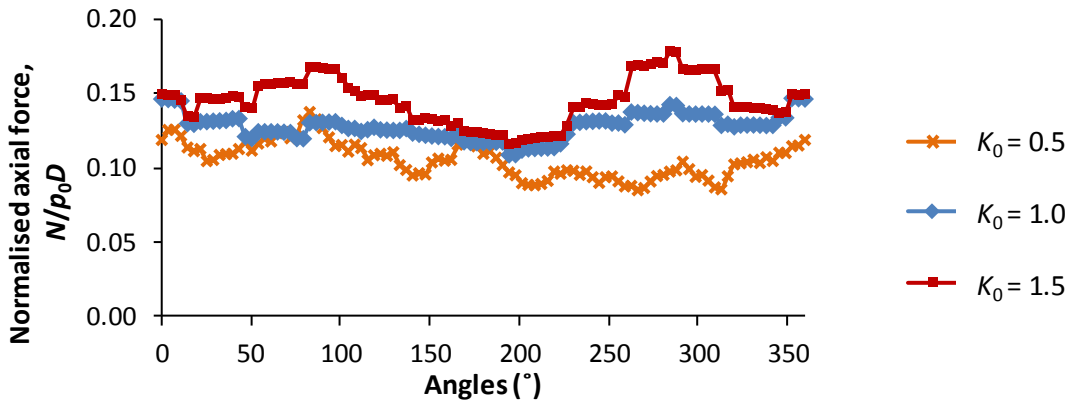


Fig. 28. Influence of in-situ stresses on lining (a) axial forces and (b) bending moments (4m bolt length, 15° bolt spacing, 10 cm lining) (correction procedures of bending moment for polygonal approximation of circular opening are referred to Boon (2013))

## Appendix A –solution for bolt support from Carranza-Torres (2009)

The equations of the analytical solution are provided in Carranza-Torres (2009), and are not reproduced here. The solution requires two dimensionless variables as input, namely  $\alpha$  and  $\beta$ , defined as:

$$\alpha = \frac{n_b A_b}{2\pi a s_l} \quad (\text{A.1})$$

$$\beta = \frac{\alpha E_b}{2G} \quad (\text{A.2})$$

where  $n_b$  is the number of rock bolts assuming that the bolt pattern covers the entire circumference,  $a$  is the opening radius,  $s_l$  is the bolt spacing in the longitudinal direction of the tunnel (tunnel axis),  $A_b$  is the cross-sectional area of the bolt,  $E_b$  is the Young's modulus of the bolt, and  $G$  is the shear modulus of the rock mass.

Substituting  $\alpha$  into  $\beta$ , we obtain:

$$\begin{aligned} \beta &= \left( \frac{n_b A_b}{2\pi a s_l} \right) \frac{E_b}{2G} \\ &= \left( \frac{n_b}{2\pi a s_l} \right) \frac{\left( \frac{E_b A_b}{L_b} \right) L_b}{2G} \\ &= \left( \frac{1}{s_\theta s_l} \right) \frac{K_a L_b}{2G} \\ &= \left( \frac{1}{s_\theta s_l} \right) \frac{K_a s_{mean}}{2G} \end{aligned} \quad (\text{A.3})$$

where  $s_\theta$  is the bolt spacing in the circumferential direction,  $L_b$  is the characteristic length of the bolt put into tension across the rock discontinuities (or the mean distance between reinforced rock joints along the bolt direction),  $s_{mean}$  is the mean rock discontinuity spacing, and  $K_a$  is the bolt stiffness acting across a rock joint which can be derived experimentally based on the procedures recommended by Stillborg (1994). Note that the assumption of  $E_b A_b = K_a s_{mean}$  is conceptually

consistent with the equations that are used in Goodman (1989) to derive the deformability of a jointed rock mass from knowledge of the rock joint stiffness (Eqs. (6) and (7)). In order to calculate the bolt forces from Eq. (15) in Carranza-Torres (2009), we replaced the group  $\beta A_b / \alpha$  with  $\frac{K_a s_{\text{mean}}}{2G}$ .

## References (Appendix A)

- Carranza-Torres, C. (2009). Analytical and numerical study of the mechanics of rockbolt reinforcement around tunnels in rock masses. *Rock Mechanics and Rock Engineering*, 42(2), 175-228.
- Goodman, R. E. (1989). *Introduction to Rock Mechanics* (2 ed.): John Wiley & Sons.
- Stillborg, B. (1994). *Professional users handbook for rock bolting* (2 ed.): Trans Tech Publications, Limited.

## APPENDIX B - SOLUTION FOR AXIAL FORCES OF LINING UNDER ISOTROPIC PRESSURE

The expressions to calculate the axial lining forces are hereafter derived. For an elastic medium of shear modulus,  $G$ , subjected to isotropic pressure,  $p_0$ , under plane-strain conditions the radial displacements for an opening of radius,  $a$ , can be calculated through the expression:

$$\frac{\Delta u_{\text{ground}}}{a} = \frac{p_0 - \Delta p}{2G} \quad (\text{B.1})$$

where  $\Delta u_{\text{ground}}$  is the radial displacement and  $\Delta p$  is the internal support pressure. The hoop strain of a thin-walled cylinder subjected to an external pressure is:

$$\varepsilon_{\theta\theta} = \frac{a\Delta p}{E_L t} (1 - \nu_L^2) \quad (\text{B.2})$$

where  $t$  is the thickness,  $E_L$  is the Young's modulus and  $\nu_L$  is the Poisson's ratio of the cylinder. The radial displacement of the lining,  $\Delta u_{\text{lining}}$ , can then be calculated as:



$$\frac{\Delta u_{lining}}{a} = \frac{a\Delta p}{E_L t} (1 - \nu_L^2) \quad (B.3)$$

In the algorithm to model lining support, the pressure exchanged between the lining and the ground is calculated from the penetration distance,  $\Delta u_{node}$ , of the lining nodes into the ground (see Fig. B1). The penetration distance can be expressed as:

$$\frac{\Delta u_{node}}{a} = \frac{\Delta p}{K_L a} \quad (B.4)$$

Where  $K_L$  is the contact stiffness between the ground and lining. The displacements have to satisfy the following compatibility equation:

$$\frac{\Delta u_{ground}}{a} = \frac{\Delta u_{lining}}{a} + \frac{\Delta u_{node}}{a} \quad (B.5)$$

Combining the equations and ignoring  $\nu_L^2$  to be consistent with the DEM models, we obtain:

$$\Delta p = \frac{p_0 E_L t K_L}{2 K_L G a + \frac{2 E_L t G}{a} + E_L t K_L} \quad (B.6)$$

Then, knowing that  $N = a\Delta p$ , we can deduce the expression for the axial force provided in Eq. (13)

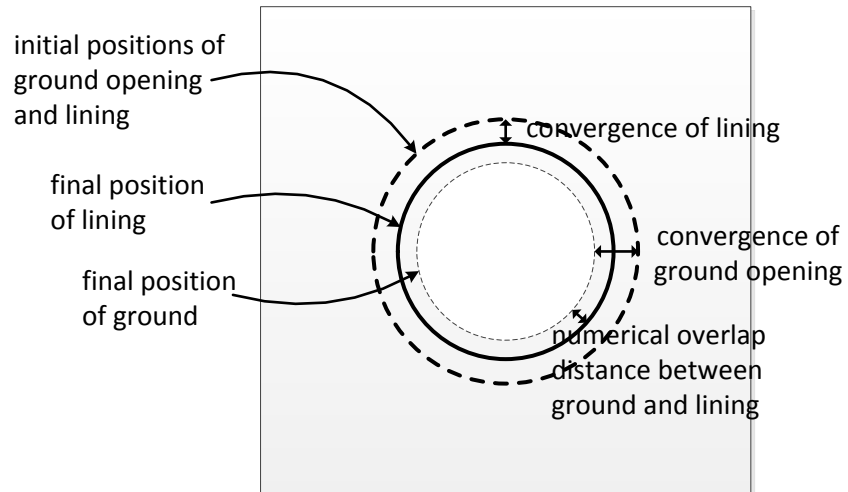


Fig. B1. Schematic showing the significance of lining-rock interface compliance